Beyond GWTC-3: Analysing and verifying new gravitational-wave events from community catalogues

Daniel Williams

SUPA, School of Physics & Astronomy, University of Glasgow, G12 8QQ

April 2025

Abstract. The public release of data from the LIGO and Virgo detectors has enabled the identification of potential gravitational wave signals by independent teams using alternative methodologies. In addition to the LIGO-Virgo-KAGRA (LVK) collaboration's GWTC-3 catalogue there have been several additional works claiming the detection of signals in the data from the first three observing runs. In this paper we present an analysis of these new signals using the same analysis workflow which was used to generate the GWTC-2.1 and GWTC-3 catalogues published by the LVK, matching the analysis configuration as closely as possible, and we provide our parameter estimation results in a format comparable to those of the GWTC-3 data release for 57 events not previously analysed in LVK analyses. We find our results to be broadly consistent with those published by other groups. We also include a discussion of the workflow developed for this analysis.

1. Introduction

As the result of rapid developments in detector technology and data analysis techniques, the field of gravitational wave detection has advanced from the first detection of a signal, GW150914_095045 [1], from a binary black hole, in 2015, to frequent and routine observation of binary black hole coalescence (BBH) signals. This has allowed the creation of catalogues of observed signals, with four of these catalogues having been produced to date by the LIGO-Virgo-KAGRA collaborations (LVK) [2–5].

Gravitational wave signals are detected in a low signal-to-noise regime, and signals are generally short compared to the total observing time. The needle-in-a-haystack-like problem of detecting signals currently necessitates performing analysis of the data in at least two stages. In the first of these stages signals are identified by *searches* of the data, for example [6–9]. Searches identify candidate signals in the detector data, estimate the significance of the event, and provide an estimate of some of the astrophysical parameters of the system which produced the signal. The significance can either be calculated statistically, as the false alarm rate of the candidate, or by attempting to estimate the probability that the candidate had an astrophysical origin [10, 11].

The second stage uses statistical inference techniques to perform model selection on signals identified in the search stage. This stage is referred-to as parameter estimation (PE), and provides more detailed and comprehensive analysis of the signal, examining only the data in a short time window around the signal. The PE stage is generally computationally intensive, using Markov chain Monte Carlo techniques to determine posterior distributions in a Bayesian framework such as LALInference [12] or Bilby [13], and may require thousands of core hours to complete. Alternative approaches to this problem are in active development. These include approaches which reduce the complexity of the inference problem, for example Cogwheel [14], as well as approaches which use machine learning, such as Vitamin [15] and Dingo [16].

The events reported in these catalogues therefore fall into two sets; a full list of possible events which have been identified by a search, which may number in the thousands of candidates; and a much shorter list of candidates which have been analysed in greater detail using PE techniques to determine the properties of the astrophysical source. This shorter list is generally created by applying a threshold to some measure of the signals' significance. The method used to perform the search can affect the calculation of the false alarm rate for each trigger, thus by either choosing a different cut, or using a different search methodology it is possible to produce different event lists for further analysis.

The most complete catalogue produced by the LVK to date is GWTC-3 [5], which includes results from the first three observing runs of the ground-based detectors ‡. Data from these detectors are made publicly available at the end of a proprietary period, allowing both the reproduction of results presented in LVK publications, and the identification of signals using alternative techniques to those used by the LVK. The Open Gravitational-Wave Catalog (OGC) series [17–20] and the Institute for Advanced Studies (IAS) series [21–25] are the most extensive third-party catalogues, with each spanning the three observing runs for which data is publicly available. There are also a number of catalogues which span only a subset of the total observing time of the detectors. These catalogues have generally accompanied descriptions of either novel techniques for improving the sensitivity of existing search codes, for example pycbc-kde [26] and cWB [27]; or entirely novel search techniques such as AresGW which make use of machine learning [28]. Each of these catalogues present a different set of candidate events (although there is considerable overlap between each). The differences in the set of events identified can be a result of the efficiency at which a code can identify signals (especially at low signal-to-noise ratios), the significance statistic, and method used to calculate it for a given signal §, or a combination of the two. As a result of these various

‡ The authors note that the LVK's GWTC catalogues are cumulative, so GWTC-3 is considered to contain events from all three observing runs, and not just the most recent observing run, O3b; we have treated the OGC catalogues in the same way in this work, but the nature of IAS catalogues suggests these catalogues are not cumulative.

§ Prior to GWTC-3, LVK analyses used the false alarm rate to determine this cut [2–4]; in GWTC-3 [5] the methodology was changed to use the probability of astrophysical origin.

differences 61 events have been reported in third-party catalogues which are not present in the LVK's GWTC-3 catalogue, or its related data releases.

This work aims to provide detailed PE results for 57 of these events in the same format as those provided in the GWTC-3 data release, and produced in a way which was consistent with analyses used for that catalogue, in order to produce a consistent dataset of as many events claimed to date across the literature as possible. In preparing this work we used Asimov [29], a workflow management tool used by the LVK to produce GWTC-3, to analyse the triggers presented in third-party catalogs which were not present in the GWTC-3 PE analysis dataset, and we provide an accompanying dataset of Asimov blueprints which can be used to both reproduce these analyses, and easily configure additional analyses at scale across the extended set of events. These are further detailed in Appendix B. We were unable to produce well-converged posterior distributions using our technique for four events: GW 190704_104834, GW 190920_113516, GW 191228_085854, and GW 200316_235947 (the former two were first published in IAS-3, the latter two in IAS-4). In order to ensure reproducibility we use only publicly available software and data to perform our analysis, and we provide data in an accompanying data release to facilitate the straightforward reproduction of our results.

In section 2 we describe the approach taken to select events for consideration in this work.

In section 3 we provide a brief overview of the method used to configure and perform the new PE analyses. We discuss specifically the differences between the analyses and datasets presented in this work and the original GWTC-3 analysis in section 3.1. We present the results of these analyses, and a discussion of the differences between our results and those presented in the various third-party catalogues in section 4. Where PE results were provided in the third-party catalogue's data release, we have compared our PE results to their results. Finally, tables of estimated source parameters for each of these events are provided in Appendix A, and a technical description of the Asimov blueprints used for the analysis is contained in Appendix B.

2. Event selection

In this work we present PE results for all of the gravitational wave events which have been presented across various third-party catalogues [17–28], but which were not present in GWTC-3 [5], or which were not selected for further PE study in that work. Events identified in each catalogue's publication as being new detections were selected ‖.

The events which we provide PE for are summarised in table 1, alongside a summary of the catalogues these are contained within. The pycbc-kde catalogue

‖ A number of events were reported first in 3-OGC which were later reported in GWTC-2.1; those events have not been included in this work, as they are contained within GWTC-3. Other events may appear in some editions of third party catalogues, but were removed from later editions; we have chosen to produce PE for the maximal set of events.

present two sets, labeled "gold" and "silver" in that work; we present PE for both sets. We have attempted to perform PE on all of the events for which these additional catalogues provided PE (or all of the new significant events identified in the case of those publications which did not provide PE samples in a data release).

We did not conduct our own search as part of this work, so do not provide new estimates of the significance of the events for which we present PE.

3. Analysis Workflow

We modelled our analysis workflow closely on that presented in GWTC-3, but have made alterations where required in order to use only information which is available to the general public, and to reduce the computing resource requirements where necessary. A full description of the differences between the workflow and data products used in this work compared to GWTC-3 is contained in section 3.1.

In performing our analysis we exclusively use open source software which is publicly available, in addition to publicly available data. In addition we provide data files (in a format described in Appendix B) which allow the precise analysis workflow used to be replicated, including the acquisition of data and its analysis. These blueprint files, alongside the Asimov software, and publicly available analysis codes, are sufficient for reconstructing the entire analysis pipeline with a small number of command-line actions on an appropriate computer system. The resulting workflow will download the publicly available strain data, estimate the noise in the data segment, configure and run the parameter estimation process itself, and will then perform appropriate post-processing on results in order to create a dataset comparable to one from GWTC-3. This abstracts the process of determining the running-order of each step in the workflow, and interacting with a high-throughput computing cluster running HTCondor. This workflow management substantially reduces the amount of human intervention required in producing results from this multi-stage analyses such as the one we employed.

We used event times presented in each catalogue, or where relevant, its data release, to determine the event time at which to perform the analysis. Additionally, we used the estimate of either component masses or chirp mass for each signal to determine both a reasonable prior range for the chirp mass parameter in the analysis, and the segment length which should be analysed, based on the (2,2)-mode of the IMRPhenomXPHM waveform. The use of the (2,2)-mode was made as this mode contributes the vast majority of power to the signal, and ensuring that the segment length is sufficient to contain the entire waveform in this mode will ensure that power is not lost from the detector band. Higher modes can also contribute to the signal power, however they are only likely to be observed in a small number of binaries [30] while potentially adding considerably to the required segment length, and consequently the time required to complete the analysis. Consequently, and given the low SNR of the signals being considered we elected to only guarantee the full resolution of the (2,2)-mode. Choosing the shortest segment length which will still allow full analysis of the signal will optimise

Event	OGC				IAS					pycbc	AresGW	cwb
	1	2	3	4	1	2	3	4	HM	kde		
GW 151205_195525	·	Y	·	·	Y	Y	Y	Y	·	·	·	·
GW 151216_092416	·	·	·	·	Y	Y	Y	Y	·	·	·	·
GW 170121_212536	·	Y	Y	Y	·	Y	Y	Y	·	·	·	·
GW 170202_135657	·	·	Y	Y	·	Y	Y	Y	·	·	·	·
GW 170304_163753	·	Y	Y	Y	·	Y	Y	Y	·	·	·	·
GW 170403_230611	·	·	Y	Y	·	Y	Y	Y	·	·	·	·
GW 170425_055334	·	·	·	·	·	Y	Y	Y	·	·	·	·
GW 170727_010430	·	Y	Y	Y	·	Y	Y	Y	·	·	·	·
GW 190426_082124	·	·	·	·	·	·	·	·	·	·	Y	·
GW 190427_180650	·	·	·	Y	·	·	·	·	·	·	·	·
GW 190511_125545	·	·	·	·	·	·	·	·	·	·	Y	·
GW 190511_163209	·	·	·	·	·	·	·	·	Y	·	·	·
GW 190514_065416	·	·	·	·	·	·	·	·	·	Y	·	·
GW 190523_085933	·	·	·	·	·	·	·	·	·	·	Y	·
GW 190524_134109	·	·	·	·	·	·	·	·	Y	·	·	·
GW 190530_030659	·	·	·	·	·	·	·	·	Y	·	·	·
GW 190530_133833	·	·	·	·	·	·	·	·	Y	·	·	·
GW 190604_103812	·	·	·	·	·	·	·	·	Y	·	·	·
GW 190605_025957	·	·	·	·	·	·	·	·	Y	·	·	·
GW 190607_083827	·	·	·	·	·	·	·	·	·	·	Y	Y
GW 190614_134749	·	·	·	·	·	·	·	·	·	·	Y	·
GW 190615_030234	·	·	·	·	·	·	·	·	Y	·	·	·
GW 190705_164632	·	·	·	·	·	·	·	·	·	·	Y	·
GW 190707_083226	·	·	·	·	·	·	Y	·	Y	·	·	·
GW 190711_030756	·	·	·	·	·	·	Y	·	Y	·	·	Y
GW 190718_160159	·	·	·	·	·	·	Y	·	·	·	·	·
GW 190725_174728	·	·	·	·	·	·	·	·	·	Y	·	·
GW 190805_105432	·	·	·	Y	·	·	·	·	·	·	·	·
GW 190806_033721	·	·	·	·	·	·	·	·	Y	·	·	·
GW 190814_192009	·	·	·	·	·	·	Y	·	·	·	·	·
GW 190818_232544	·	·	·	·	·	·	Y	·	Y	·	·	·
GW 190821_124821	·	·	·	·	·	·	Y	·	·	·	·	·
GW 190904_104631	·	·	·	·	·	·	·	·	·	·	Y	·
GW 190906_054335	·	·	·	·	·	·	Y	·	Y	·	·	·
GW 190910_012619	·	·	·	·	·	·	Y	·	·	·	·	·
GW 190911_195101	·	·	·	·	·	·	·	·	Y	·	·	·
GW 190916_200658	·	·	·	·	·	·	·	·	·	Y	·	·
GW 190926_050336	·	·	·	·	·	·	·	·	·	Y	·	·
GW 191113_103541	·	·	·	·	·	·	·	·	Y	·	·	·
GW 191117_023843	·	·	·	·	·	·	·	Y	·	·	·	·
GW 191127_050227	·	·	·	·	·	·	·	·	·	Y	·	·
GW 191208_080334	·	·	·	·	·	·	·	·	·	Y	·	·
GW 191224_043228	·	·	·	Y	·	·	·	·	·	Y	·	·
GW 191228_195619	·	·	·	·	·	·	·	·	Y	·	·	·
GW 200106_134123	·	·	·	Y	·	·	·	·	·	·	·	·
GW 200109_195634	·	·	·	·	·	·	·	Y	·	·	·	·
GW 200129_114245	·	·	·	Y	·	·	·	·	·	·	·	·
GW 200208_211609	·	·	·	·	·	·	·	·	·	·	Y	·
GW 200210_005122	·	·	·	Y	·	·	·	·	·	·	·	·
GW 200210_100022	·	·	·	·	·	·	·	Y	Y	·	·	·
GW 200220_124850	·	·	·	·	·	·	·	·	·	Y	·	·
GW 200214_223307	·	·	·	·	·	·	·	·	·	·	·	·
GW 200225_075134	·	·	·	·	·	·	·	Y	·	·	·	·
GW 200301_211019	·	·	·	·	·	·	·	·	Y	Y	·	·
GW 200304_172806	·	·	·	·	·	·	·	·	Y	·	·	·
GW 200305_084739	·	·	·	Y	·	·	·	·	·	·	·	·
GW 200318_191337	·	·	·	Y	·	·	·	·	·	·	·	Y

Table 1. Events for which parameter estimation (PE) is provided in this work, and the catalogues from which they originate.

analysis time, while choosing a suitable prior over mass ratio will prevent the requirement for excessively long data segment lengths to match the length of waveforms for very low-mass systems.

These quantities were used to prepare *blueprint* files which describe each event for the Asimov workflow system. The same workflow was then applied to each event:

(i) Gravitational wave strain data were then downloaded, by Asimov, from the Gravitational-wave Open Science Centre (GWOSC) in the form of frame files.

(ii) Bayeswave [31] was run on the data surrounding the event time, and containing the signal, from the frame files in order to produce on-source PSDs for each detector. On-source PSDs provide an estimate of the noise content of data by first removing non-Gaussian features in the data before computing the PSD. In contrast, off-source PSDs use data collected before and after the signal to estimate the noise.

(iii) Bilby [13] (via Bilby_pipe [32]) was used to perform model selection with the Dynesty [33] nested sampler and the IMRPhenomXPHM [34] waveform.

(iv) PESummary [35] was used to perform post-processing on the posterior samples produced by the Bilby analysis, and produce samples for derived quantities.

We then reviewed the results for each event using plots produced by PESummary in the final step of the workflow in order to scrutinise the convergence of the samples, and identify problems with the analysis, such as situations where the posteriors railed against the priors, or where prior dominance was observed in the posterior. In cases where problems were identified a new blueprint was prepared to produce a new Bilby analysis, and then this was run using Asimov.

In order to produce the final data release, and to simplify the process of comparing our results to those of the other catalogues, we used PESummary's ability to compare sample sets, and produce "metafiles" containing multiple sets of samples. In keeping with the GWTC-3 data release we have labelled samples from our analysis as `C01:IMRPhenomXPHM`, but we have labelled the samples from the other catalogues with their respective catalogue name as used in table 1.

3.1. Differences compared to GWTC-3

While we have endeavoured to make our analyses as similar as possible to those performed for GWTC-3 there are a number of minor differences.

In this work we have used frame files which were published via GWOSC to perform the analysis. The GWTC-3 analysis was run on proprietary detector data prior to public release, using data retrieval systems which are not generally accessible. The GWOSC data products were produced from the same data source, but accessing the data in this way necessitated a slight change to the workflow in order to first retrieve the data frames containing the released strain data. The channel names in the GWOSC frame files are different to those used internally by the LVK, so this may be noted as a

difference between configuration files provided in our data release compared to those in the GWTC-3 data release.

We have used a newer version of the Bayeswave package than was used in GWTC-3 which provides a substantial improvement in performance, while still using the same underlying approach to producing on-source PSD estimates. We have also used a more recent version of the Bilby library (v2.1.1 [36]) which provides better computational performance compared to the one used for GWTC-3.

The GWTC-3 analyses marginalised over the uncertainty in detector calibration. The data to allow this marginalisation to be performed is not made publicly available by the LVK, and so we elected not to attempt to include this uncertainty. LIGO and Virgo data in observing runs 1, 2, and 3 were re-calibrated prior to release, and we did not expect the calibration uncertainty to present a large additional source of uncertainty in our analyses, especially given the low SNR of the majority of events in this work. The 4-OGC catalogue does attempt to include this uncertainty, but uses the uncertainty envelopes which were published to coincide with specific GWTC-3 events; 4-OGC events are then analysed using the calibration uncertainty for the closest published event in time, with the reasoning that the uncertainty is expected to evolve slowly over time.

For the majority of events we performed sampling directly over a cosmologically-motivated distance prior (that is, a prior on the redshift, z, which is uniform in comoving volume, V_c and source-frame time with the form

$$p(z) \propto \frac{1}{1+z}\frac{dV_c}{dz}$$

in comparison GWTC-3 reweighted its samples to this prior, having sampled over a power-law prior of the form

$$p(x) = \frac{3x^2}{x_{\rm max}^3 - x_{\rm min}^3}$$

for $x_{\rm max}, x_{\rm min}$ respectively the maximum and minimum bound of the prior over the distance, x. By performing the sampling directly from the cosmological prior we were able to achieve higher sampling efficiency and reduced the complication of the post-processing required. As a result, however, we do not provide a set of samples from a power-law prior in our data release, and our samples should be treated as comparable to the samples labelled as "cosmo" in the LVK's GWTC-3 release. A small number of events were sampled with the power-law prior, but these have been reweighted to make them comparable to the other results in this work ¶.

In order to determine the optimal prior ranges for the events in this work we often required multiple analyses, which would be reviewed, and lead to subsequent analyses which were configured to address any observed problems. GWTC-3 avoided this iterative process in part as a result of the existence of *preliminary* analyses which had

¶ An earlier iteration of this work focused only on these events, which were events newly reported in 4-OGC. When expanding the scope of the work to include a much larger number of events with a greater distribution of SNRs we chose to perform subsequent analysis with the cosmologically-motivated prior and then reweighted the previous analyses to the new prior.

been produced shortly after signals were detected. These analyses were intended to provide rough estimates of the signals' parameters in order to inform subsequent follow-up. Scrutinising the posterior distributions from these preliminary analyses allowed suitable prior ranges to be estimated. The software product for performing this analysis was not publicly available at the time that we started our analysis, and we did not have access to preliminary results to analyse with it. The tool used to perform this analysis is now publicly available as PE-Configurator [37].

The largest single difference between our analysis and that of GWTC-3 is the choice of waveform models; in our work we elected to only perform analysis using the IMRPhenomXPHM model; GWTC-3 contains samples from both IMRPhenomXPHM and SEOBNRv4PHM [38]. This choice was born out of practicality; GWTC-3 used the RIFT [39–43] pipeline to produce samples for SEOBNRv4PHM, which generally requires much more time to evaluate a single waveform than IMRPhenomXPHM. This pipeline made substantial use of both CPU and GPU acceleration resources, which were not available to us when preparing this work using a small computing resource at the Institute for Gravitational Research at the University of Glasgow. These two waveforms make use of different techniques to model signals; IMRPhenomXPHM makes use of phenomenological fits to waveforms generated by numerical relativity simulation, whereas SEOBNRv4PHM uses an effective one-body approximation which is calibrated against simulations. As a result we are also unable to provide "mixed" samples for these events in a similar format to those in the LVK's GWTC-3 data release. (Mixed samples are produced by combining a random selection of points from the posterior distributions from multiple analyses which have compatible prior distributions. In the GWTC-3 data release these are constructed such that half of the points in the mixed sample set were produced using the IMRPhenomXPHM waveform, and half from the SEOBNRv4PHM model.)

We used the Planck15 cosmology from astropy [44, 45] when determining source-frame quantities, where GWTC-3 use a slightly different set of values to form their cosmology based on values in LALInference [12] (we use $H_0 = 67.74\text{km/Mpc/s},\ \Omega_\text{m} = 0.3075$, whereas GWTC-3 use $H_0 = 67.90\,\text{km/Mpc/s},\ \Omega_\text{m} = 0.3065$).

4. Source properties

Here we present the properties of the various events reported in the community catalogues, and compare them to the results which were presented in those catalogues. Due to the large number of events, we have divided these between each of the three observing runs.

In order to quantitatively compare the posterior probability distributions between our analyses and those from the other catalogues we calculate the Jensen-Shannon (JS) divergence between the marginal distributions for a selection of source properties. The JS divergence is derived from the Kullback-Leibler (KL) divergence, but is symmetrised

and hence bounded. It is defined

$$\mathrm{JSD}(A||B) = \frac{\mathrm{KL}(A||M) + \mathrm{KL}(B||M)}{2} \tag{1}$$

where A and B are probability distributions, $M = (A + B)/2$, and KL is the KL divergence [46] between A and B:

$$\mathrm{KL}(A||B) = \int_{-\infty}^{\infty} A(x) \log \frac{A(x)}{B(x)} \mathrm{d}x \tag{2}$$

When the logarithm in equation 2 is the natural logarithm the JSD will have a range of $[0\,\mathrm{nat}, \ln 2 \approx 0.69\,\mathrm{nat}]$. A value of 0 implies the distributions are identical, while distributions with a JD divergence of $\ln 2\,\mathrm{nat}$ have no similarity. Examples of different distributions and their JS divergences are shown in figure 1, including instances where the divergence is minimal and maximal. Analyses do not directly produce posterior probability distributions, but rather produce samples drawn from the distribution. In order to calculate the JS divergence we first calculate a Gaussian kernel density estimate from the samples which is used to evaluate equation 1.

While the data release which accompanies this publication provides posterior probability distributions on all of the parameters included in GWTC-3 and its data release, we have chosen to show an illustrative subset of the source parameters in this work.

These are:

- chirp mass, a reduced mass of the binary system, defined as

  $$\mathcal{M} = \frac{(m_1 m_2)^{3/5}}{(m_1 + m_2)^{1/5}}$$

  for m_1 and m_2 the mass of the primary and secondary component of the binary respectively.
- mass ratio, $q = m_2/m_1$
- the effective spin parameter,

  $$\chi_{\mathrm{eff}} = \left[\frac{m_1 \chi_{1,\perp} + m_2 \chi_{2,\perp}}{m_1 + m_2}\right]$$

  where $\chi_i = cS_i/(Gm_i^2)$ is the dimensionless component spin for the i-th component, with S_i, the magnitude of the total spin vector of the i-th component, and $\chi_{i,\perp}$ is the component of this dimensionless component spin which is perpendicular to the direction of the Newtonian orbital angular momentum vector. A non-zero value for this parameter indicates support for spins being present within the system; if positive this indicates the components' spins are aligned, and if negative that they are anti-aligned.
- the precessing spin parameter,

  $$\chi_{\mathrm{p}} = \max\left[\chi_{1,\perp}, \frac{q(4q+3)}{4+3q}\chi_{2,\perp}\right]$$

  This component provides a measure of the spin precession present in the binary.

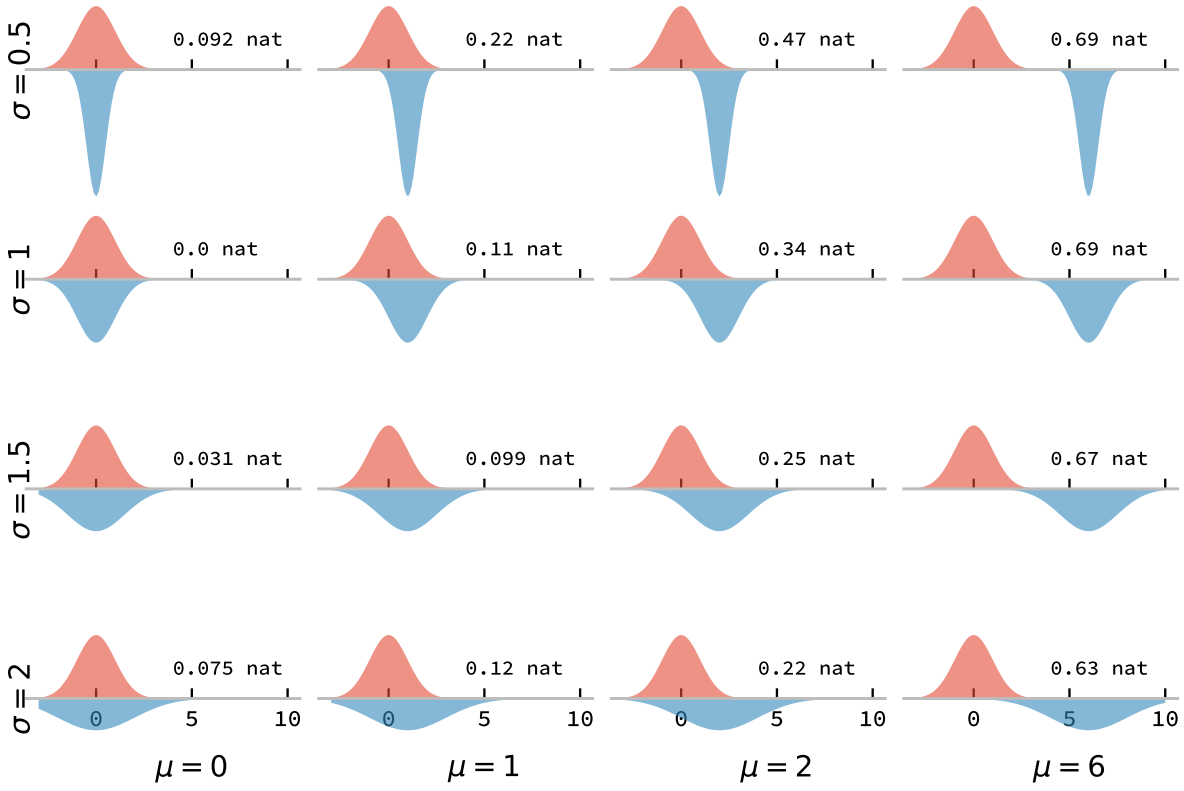

Figure 1. A selection of normal distributions with differing means (μ) and standard deviations (σ). In each case the red distribution above the x-axis has $\mu = 0$ and $\sigma = 1$. The blue distribution below the axis have $\mu = (0, 1, 2, 6)$ in each plot in the first, second, third, and fourth column respectively, counting from the left; and $\sigma = 0.5, 1, 1.5$, and 2 for the first, second, third, and fourth row, counting from the bottom. To the right of each pair of distributions the Jensen-Shannon Divergence between the distribution is shown in units of nat.

	2-OGC					IAS-1				
Event	$\mathcal{M}_{\rm src}$	q	$\chi_{\rm eff}$	$\chi_{\rm p}$	$D_{\rm L}$	$\mathcal{M}_{\rm src}$	q	$\chi_{\rm eff}$	$\chi_{\rm p}$	$D_{\rm L}$
GW 151205_195525	0.010	0.004	0.001	0.001	0.008	−−	−−	−−	−−	−−
GW 151216_092416	0.016	0.032	0.010	0.009	0.042	0.127	0.263	0.413	−−	0.050

Table 2. The Jensen-Shannon divergences, in nats, between the posteriors presented in this work and those from the 2-OGC and IAS-2 data releases for the marginal posterior distributions shown in figure 2.

In each case we quote values and present probability distributions for frame-dependent parameters in the source reference frame, indicated by a subscript "src" in the parameter symbol.

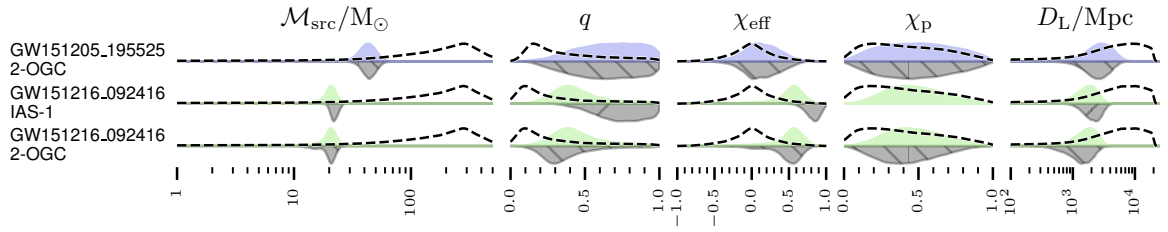

Figure 2. Violin plots showing the marginal probability distribution of a selection of inferred parameters for each signal from O1. From left to right these are the chirp mass, $\mathcal{M}_{\rm src}$ (in the source frame); the mass ratio; the effective dimensionless spin parameter, $\chi_{\rm eff}$; the precessing dimensionless spin parameter, $\chi_{\rm p}$; and the luminosity distance, $D_{\rm L}$. The coloured distributions above the x-axis represent the posterior probability distributions from our analysis, while those in grey below the x-axis are the posterior probability distributions reported in third-party catalogues. The distribution outlined by a dashed black line represents the prior probability distribution used in the analyses performed for this work. Where PE samples are presented in multiple catalogues we present the comparison between our results and each catalogue's samples, with the catalogue noted beneath the name of the event, with our results repeated in each plot.

4.1. Observing Run 1

GWTC-3 contains three events from the first observing run, all of which are binary black hole (BBH) coalescences, and include the first observed gravitaional wave event, GW 150914_095045. Two additional events have been claimed in the literature, GW 151205_195525 was reported in 2-OGC, however it was later excluded from 3-OGC, and does not appear in subsequent OGC catalogues, as changes to the search algorithm result in the signal no longer exceeding this catalogue's significance threshold. It does not appear in any of the other catalogues we considered in this work.

GW 151216_092416 was reported in IAS-1, but has not been identified as a significant trigger by any of the other catalogues we considered in this work. We note that the analyses presented in [47] used an aligned-spin waveform model, so we are unable to compare posterior distributions on the precessing spin parameter. This event has been the result of some discussion in the literature, with some authors noting [48] that analysis of this event is strongly affected by the choice of prior in the analysis. The authors of [49] question the astrophysical nature of the signal, though [50] support it. This prior-dependence appears to be reflected in our analysis: our posterior distributions diverge substantially from those presented in [21], especially in the effective spin.

We present the results of our analysis of these events for a subset of parameters in table A1, and a summary plot of the marginal posteriors for a selection of source parameters of each of these O1 events in figure 2; results from this work are shown as the distribution above the x-axis, and those from the IAS-2 and 2-OGC data releases below. Additionally, table 2 shows the Jensen-Shannon divergence for each parameter depicted in this figure.

Results from both of these publications use a different waveform family to produce results from those used in this work. The results from 2-OGC were created with the IMRPhenomPv2 [51], in contrast to those from both this work and 4-OGC which used IMRPhenomXPHM. Further, the results from IAS-2 use the IMRPhenomD [52] waveform, which is non-precessing. As a result we would anticipate some amount of divergence between these results and ours given the reduction in physics modelled in each of these waveforms. Further, as inference performed with IMRPhenomD necessarily cannot measure precessing spin, posteriors for $\chi_{\rm p}$, the precessing dimensionless spin parameter, are not present for results derived from IMRPhenomD. Results from IAS-2 were not sampled using a prior which was uniform in comoving volume as those from this work were, so we have reweighted these posteriors to represent draws with the same prior, and rejection-sampled the resulting weighted samples. This was performed using the PESummary library.

4.2. Observing Run 2

In addition to the eight gravitational-wave event candidates reported in GWTC-3, both IAS-2 and 2-OGC claim novel events, with additional events being identified in 3-OGC and 4-OGC. We compare the results of our analyses to PE results available from each group for O2 events, 2-OGC, 4-OGC, and IAS-2; as with the events in O1, there is a difference in the waveforms used for sampling between each of these catalogues, and the IAS-2 results have been reweighted to account for the differing luminosity distance priors. We present the median estimates of a subset of the source parameters in table A1.

In figure 3 we present marginal posteriors for the six O2 events from 4-OGC, and 11 from IAS-2. The JS divergence between our posteriors and those in each data release are contained in table 3.

The largest divergence appears in GW 170202_135657 where the inferred source chirp mass has a divergence of 0.058 nat between our results and the IAS-2 results. The IAS-2 results show a degree of bimodality which is not seen in the 2-OGC, 4-OGC, or our own results. Similarly, the IAS-2 posterior for GW 170403_230611 shows support for extremal, negative $\chi_{\rm eff}$. Our results show some support for negative $\chi_{\rm eff}$ compared to our prior, this is much less pronounced, and is comparable to the results from the two OGC publications. It is unclear where the source of this difference arises. The primary difference between results produced here and in the OGC catalogues, and those produced in the IAS catalogues are the parameter estimation codes themselves.

4.3. Observing Run 3

The third observing run saw substantially improved sensitivity from all three gravitational detectors, and a much greater network duty cycle, with one detector observing around 96% of the time in O3 [5] compared to 42.8% in O1 and 46% in O2 [53]. As a result an order of magnitude more events are reported in GWTC-3 from

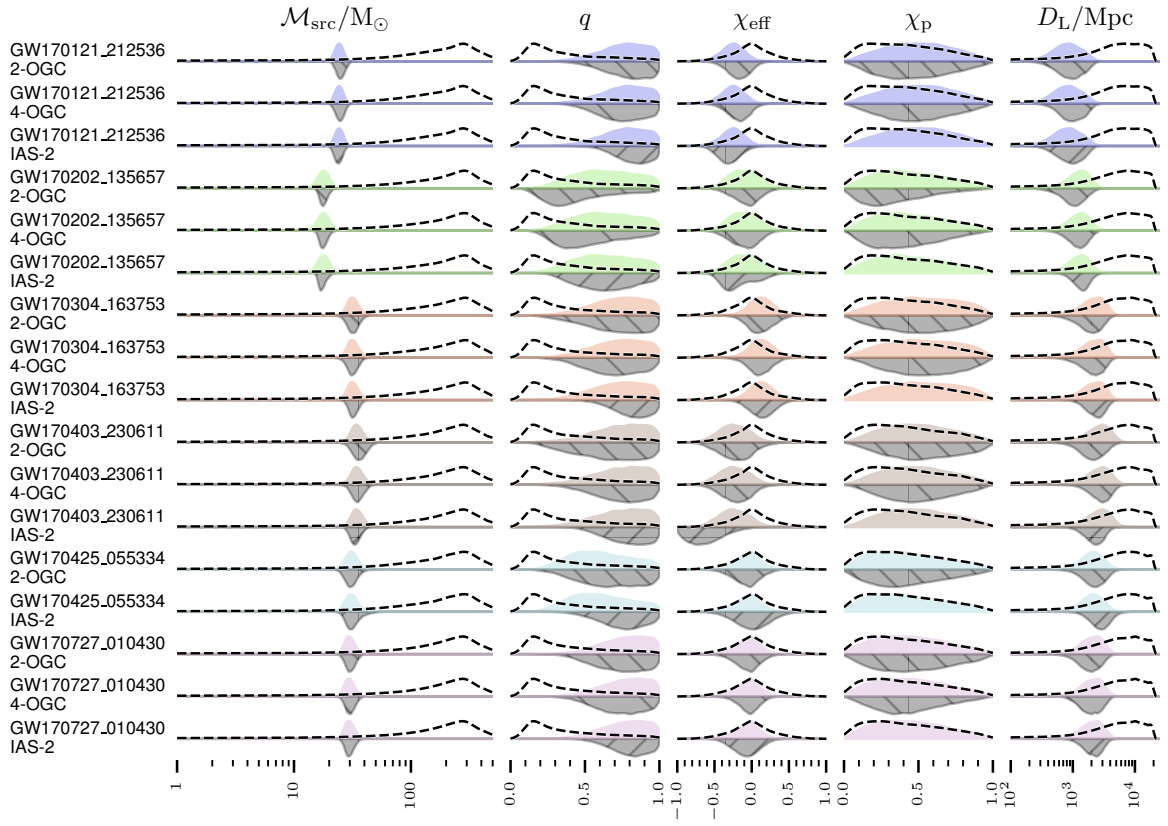

Figure 3. Violin plots showing the marginal probability distribution of a selection of inferred parameters for each signal from O2. The parameters displayed, and the prior and posterior quantities depicted in various parts of each plot are the same as in figure 2. Where PE samples are presented in multiple catalogues we present the comparison between our results and each catalogue's samples, with the catalogue noted beneath the name of the event.

this period. Similarly other catalogues which search and analyse this data find far more candidate events than in O1 and O2 combined.

As a result in the plots and tables which follow we divide results between the two parts of the observing run as defined by the LVK's GWTC-2.1 and GWTC-3 catalogues, into O3a and O3b, however we present the median inferred source parameters for the same subset of parameters as in table A1 for all O3 events in table A2. A similar divide is present with some of the other catalogues; events from O3a are described by IAS-3, and O3b by IAS-4. Both parts are considered in 4-OGC (which updates 3-OGC, which describes events from only O3a), IAS-HM, pycbc-kde, AresGW, and cWB. A substantially greater variety of catalogues and techniques cover this period, though only 3-OGC, 4-OGC, IAS-3, IAS-4, and IAS-HM provide publically available data releases of their PE results. Given the similarity between the setup used in both 3-OGC and 4-OGC we have elected to consider only 4-OGC results, as these include all of the events contained within 3-OGC.

The results of the various O3a analyses are depicted in figure 4 and those for O3b

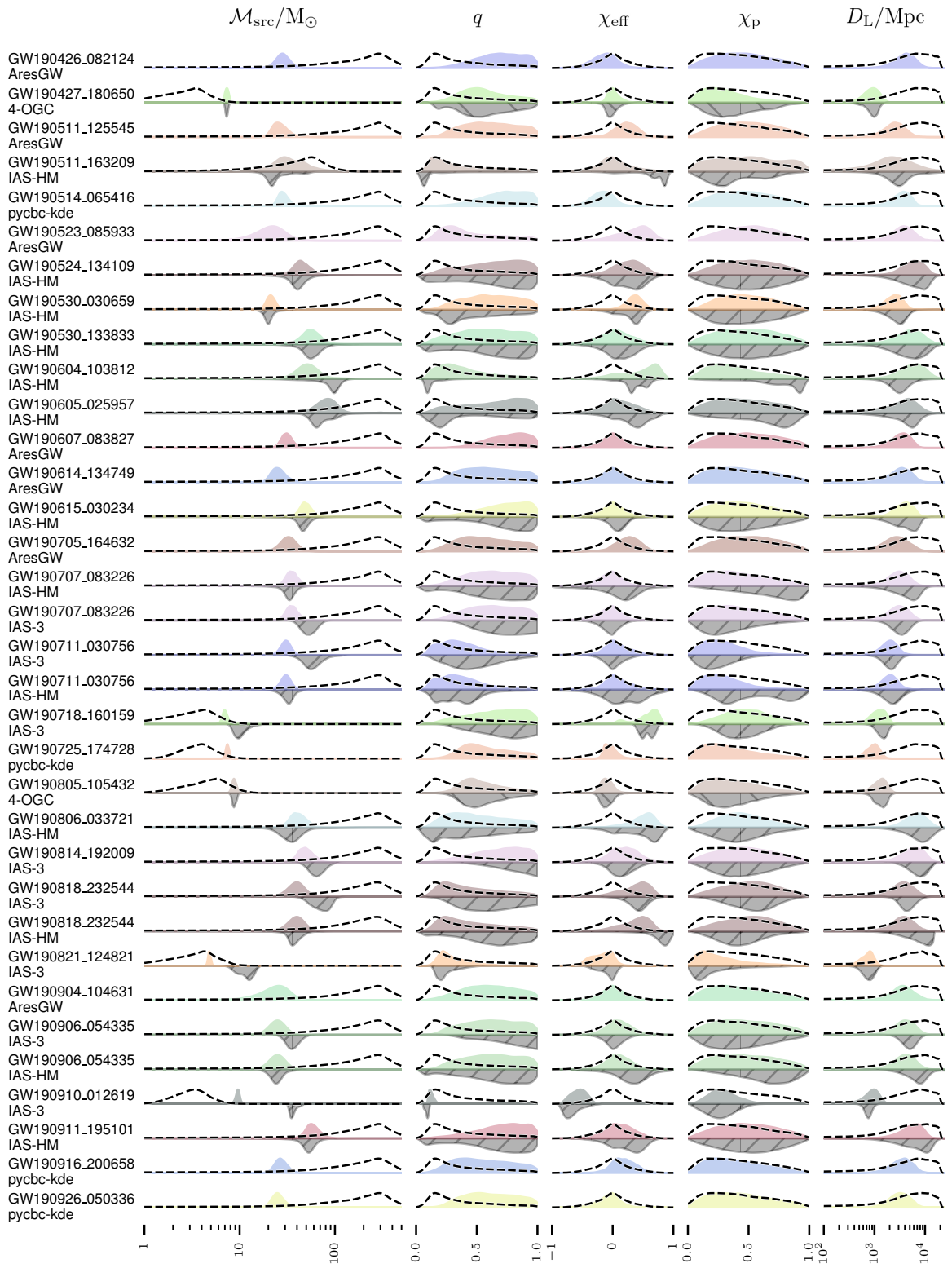

Figure 4. Violin plots showing the marginal probability distribution of a selection of inferred parameters for each signal from O3a. The parameters displayed, and the prior and posterior quantities depicted in various parts of each plot are the same as in figure 2. Where PE samples are presented in multiple catalogues we present the comparison between our results and each catalogue's samples, with the catalogue noted beneath the name of the event.

Event	2-OGC					4-OGC				
	$\mathcal{M}_{\rm src}$	q	$\chi_{\rm eff}$	$\chi_{\rm p}$	$D_{\rm L}$	$\mathcal{M}_{\rm src}$	q	$\chi_{\rm eff}$	$\chi_{\rm p}$	$D_{\rm L}$
GW 170121_212536	0.018	0.002	0.036	0.003	0.007	0.008	0.002	0.033	0.001	0.029
GW 170202_135657	0.045	0.089	0.008	0.025	0.026	0.046	0.032	0.002	0.003	0.014
GW 170304_163753	0.001	0.004	0.002	0.000	0.011	0.003	0.004	0.003	0.002	0.009
GW 170403_230611	0.017	0.020	0.004	0.003	0.033	0.004	0.002	0.004	0.001	0.007
GW 170425_055334	0.001	0.015	0.001	0.000	0.003	−−	−−	−−	−−	−−
GW 170727_010430	0.005	0.005	0.001	0.001	0.008	0.004	0.005	0.003	0.003	0.004

Event	IAS-2				
	$\mathcal{M}_{\rm src}$	q	$\chi_{\rm eff}$	$\chi_{\rm p}$	$D_{\rm L}$
GW 170121_212536	0.004	0.034	0.013	−−	0.012
GW 170202_135657	0.058	0.006	0.024	−−	0.028
GW 170304_163753	0.018	0.055	0.002	−−	0.032
GW 170403_230611	0.021	0.022	0.269	−−	0.045
GW 170425_055334	0.012	0.094	0.036	−−	0.069
GW 170727_010430	0.005	0.017	0.006	−−	0.007

Table 3. The Jensen-Shannon divergences, in nats, between the posteriors presented in this work and those from the 2-OGC, 4-OGC, and IAS-2 data releases for the marginal posterior distributions shown in figure 3.

are shown in figure 5; events from pycbc-kde and AresGW show only our marginal posteriors.

The cWB catalogue does not include any events which are not reported in another catalogue, so these are not depicted separately. The JS divergences corresponding to the marginal posterior distributions shown in figure 4 are contained in table 4, while those for figure 5 are in table 5.

Similarly to results from O2, our results generally show less support for extremal binary configurations compared to results from the IAS-3 catalogue, but also show very large divergences between estimates of the chirp mass in the source frame. There is considerable overlap between the event lists from GWTC-3 and 4-OGC in O3a, and as a result we compare results between only two events from this catalogue. Neither show a large divergence between marginal posteriors. There are a larger number of events not identified in GWTC-3 from O3b, and we find good agreement between our results and those in 4-OGC for all events with GW 200210_005122 having the largest disagreement as evidenced by the JS divergence of 0.053 nat between the two source chirp mass posterior distributions, and 0.083 nat between the luminosity distance posteriors indicating only a small difference between the two results.

The IAS-4 results are broadly comparable to ours, though some other differences stand out, such as the multimodality present in the IAS-4 estimate of GW 200210_10022 which is not present in our posterior distributions.

The IAS-HM catalogue present their PE results using the IMRPhenomXODE [54] waveform model, but also provide PE results using the IMRPhenomXPHM model. We

Event	4-OGC					IAS-3				
	$\mathcal{M}_{\rm src}$	q	$\chi_{\rm eff}$	$\chi_{\rm p}$	$D_{\rm L}$	$\mathcal{M}_{\rm src}$	q	$\chi_{\rm eff}$	$\chi_{\rm p}$	$D_{\rm L}$
GW 190427_180650	0.040	0.010	0.022	0.029	0.024	−−	−−	−−	−−	−−
GW 190707_083226	−−	−−	−−	−−	−−	0.467	0.033	0.007	0.013	0.017
GW 190711_030756	−−	−−	−−	−−	−−	0.590	0.049	0.017	0.009	0.009
GW 190718_160159	−−	−−	−−	−−	−−	0.659	0.015	0.113	0.016	0.052
GW 190805_105432	0.008	0.002	0.001	0.003	0.009	−−	−−	−−	−−	−−
GW 190814_192009	−−	−−	−−	−−	−−	0.220	0.054	0.007	0.004	0.039
GW 190818_232544	−−	−−	−−	−−	−−	0.490	0.074	0.026	0.011	0.062
GW 190821_124821	−−	−−	−−	−−	−−	0.693	0.042	0.048	0.015	0.007
GW 190906_054335	−−	−−	−−	−−	−−	0.377	0.053	0.032	0.005	0.057
GW 190910_012619	−−	−−	−−	−−	−−	0.693	0.430	0.086	0.012	0.175

Event	IAS-HM				
	$\mathcal{M}_{\rm src}$	q	$\chi_{\rm eff}$	$\chi_{\rm p}$	$D_{\rm L}$
GW 190427_180650	0.040	0.445	0.022	0.029	0.024
GW 190511_163209	0.115	0.188	0.315	0.042	0.067
GW 190524_134109	0.043	0.020	0.007	0.001	0.027
GW 190530_030659	0.053	0.059	0.049	0.006	0.033
GW 190530_133833	0.023	0.022	0.010	0.000	0.010
GW 190604_103812	0.271	0.260	0.116	0.217	0.131
GW 190605_025957	0.059	0.093	0.075	0.050	0.013
GW 190615_030234	0.054	0.034	0.021	0.000	0.053
GW 190707_083226	0.049	0.025	0.149	0.114	0.103
GW 190711_030756	0.066	0.006	0.086	0.141	0.034
GW 190806_033721	0.092	0.033	0.050	0.006	0.030
GW 190818_232544	0.027	0.081	0.297	0.021	0.165
GW 190906_054335	0.029	0.024	0.137	0.051	0.141
GW 190911_195101	0.061	0.026	0.036	0.001	0.062

Table 4. The Jensen-Shannon divergences, in nats, between the posteriors presented in this work and those from the 4-OGC, IAS-3, and IAS-HM data releases for the marginal posterior distributions shown in figure 4.

use these results from their data release produced using the same prior configuration to the one used here for the posteriors labelled as IAS-HM in figure 4 and table 4. There is considerable variety in the divergences between our and their posteriors; GW 190511_163209 shows perhaps the most dramatic difference, with the IAS-HM results favouring very high effective spin (though with a bimodal distribution), while our posteriors largely reproduce the prior distribution on this parameter. Again, we note that the primary difference between the means the two results were produced are the parameter estimation codes themselves.

By construction, the events presented in this work are generally of low signficance, having failed to reach the significance threshold of at least GWTC-3. Our confidence that the signals presented here are the result of astrophysical events should consider this. However, if real, a number of these signals stand out as unusual. GW 190523_085933, GW 190718_160159, GW 190718_160159, GW 191113_103541, and GW 200210_100022

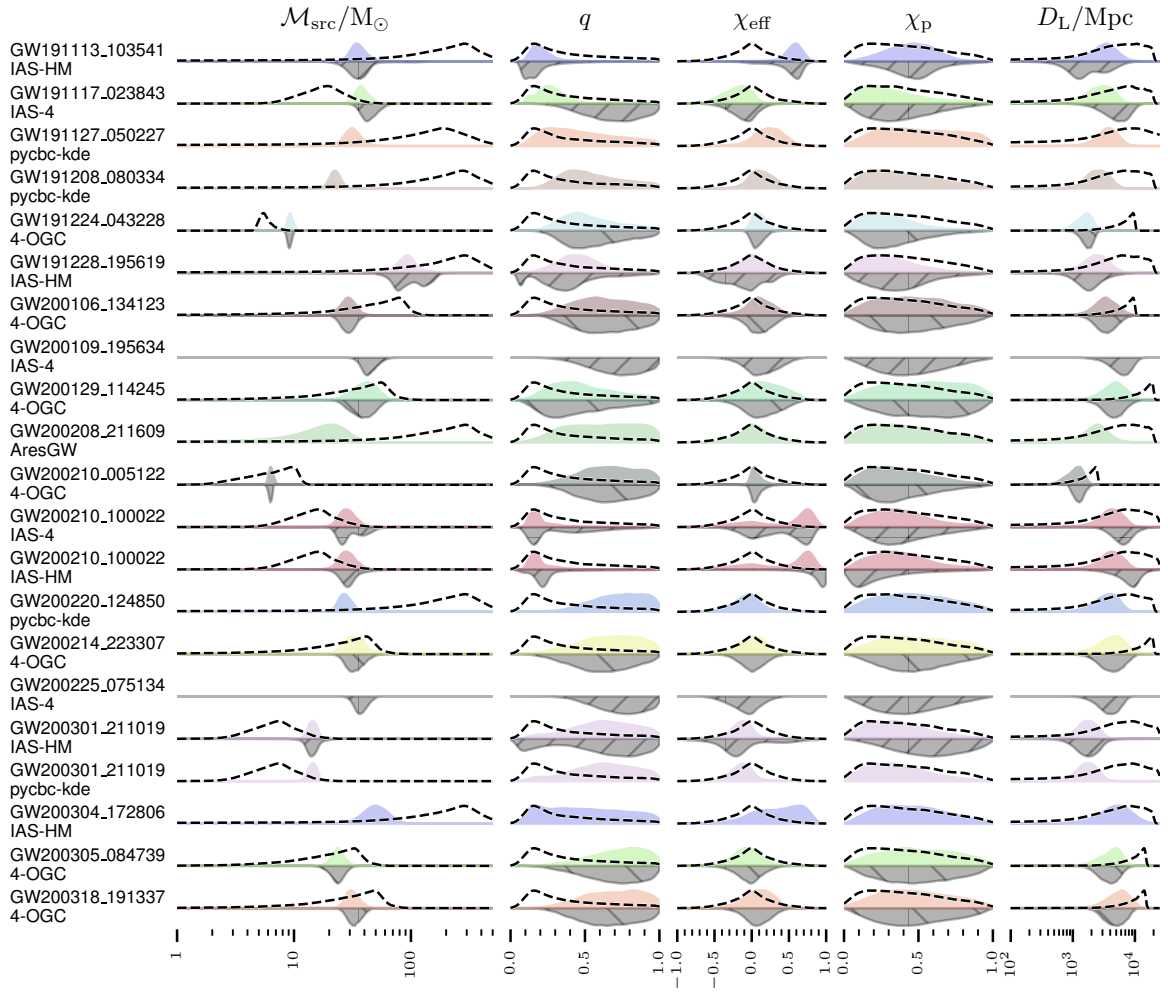

Figure 5. Violin plots showing the marginal probability distribution of a selection of inferred parameters for each signal from O3b. The parameters displayed, and the prior and posterior quantities depicted in various parts of each plot are the same as in figure 2. Where PE samples are presented in multiple catalogues we present the comparison between our results and each catalogue's samples, with the catalogue noted beneath the name of the event.

each show evidence for high positive $\chi_{\rm eff}$, while GW 190910_012619 shows strong support for high negative $\chi_{\rm eff}$ indicating an anti-aligned spin configuration.

High positive $\chi_{\rm eff}$ has previously been reported for candidates in GWTC-3, e.g. GW 190517_055101 and GW 190403_051519, but it does not contain any events with such clearly negative $\chi_{\rm eff}$. Large negative $\chi_{\rm eff}$ can be a strong indication that the binary system formed as the result of dynamical interaction [55]. However, very high spin values are also inferred when analysing non-stationary noise artefacts (glitches) under the assumption that they represent compact binary signals [56].

Event	4-OGC					IAS-4				
	$\mathcal{M}_{\rm src}$	q	$\chi_{\rm eff}$	$\chi_{\rm p}$	$D_{\rm L}$	$\mathcal{M}_{\rm src}$	q	$\chi_{\rm eff}$	$\chi_{\rm p}$	$D_{\rm L}$
GW 191117_023843	−−	−−	−−	−−	−−	0.125	0.503	0.037	0.017	0.170
GW 191224_043228	0.023	0.006	0.005	0.009	0.042	−−	−−	−−	−−	−−
GW 200106_134123	0.003	0.002	0.002	0.003	0.005	−−	−−	−−	−−	−−
GW 200109_195634	−−	−−	−−	−−	−−	0.006	0.006	0.011	0.003	0.014
GW 200129_114245	0.676	0.433	0.158	0.128	0.409	−−	−−	−−	−−	−−
GW 200210_005122	0.053	0.002	0.002	0.002	0.083	−−	−−	−−	−−	−−
GW 200210_100022	−−	−−	−−	−−	−−	0.069	0.132	0.036	0.003	0.123
GW 200214_223307	0.007	0.008	0.005	0.007	0.022	−−	−−	−−	−−	−−
GW 200225_075134	−−	−−	−−	−−	−−	0.116	0.002	0.000	0.001	0.066
GW 200305_084739	0.004	0.005	0.006	0.001	0.010	−−	−−	−−	−−	−−
GW 200318_191337	0.015	0.003	0.006	0.001	0.031	−−	−−	−−	−−	−−

Event	IAS-HM				
	$\mathcal{M}_{\rm src}$	q	$\chi_{\rm eff}$	$\chi_{\rm p}$	$D_{\rm L}$
GW 191113_103541	0.040	0.091	0.041	0.008	0.098
GW 191228_195619	0.072	0.060	0.031	0.014	0.027
GW 200109_195634	0.034	0.025	0.307	0.012	0.099
GW 200210_100022	0.030	0.107	0.193	0.070	0.201
GW 200301_211019	0.035	0.035	0.107	0.105	0.009

Table 5. The Jensen-Shannon divergences, in nats, between the posteriors presented in this work and those from the 4-OGC, IAS-4, and IAS-HM data releases for the marginal posterior distributions shown in figure 5.

5. Conclusion

In this work we examined 57 gravitational wave events which have been reported in publications by authors outside the LIGO, Virgo, and KAGRA collaborations. We have performed parameter estimation (PE) on each of these events using an analysis workflow which is as close as reasonably practicable to the one used in the preparation of the GWTC-3 catalogue, with the aim of providing a consistent dataset which encompasses all of these catalogues.

Many of the examined events were excluded from at least one other catalogue due to their not exceeding a significance threshold. The large number of such events indicates that there is a genuine requirement for a means of determining event significance which is independent of the search pipeline identifying the event. Previous approaches to this problem include [57] which was applied to GW 151216_092416 in [58], but such a metric would need to be calculated for all events from PE in order to allow construction of a catalogue which is search agnostic.

We have identified divergence between the results presented in the IAS catalogue publications which were produced with the Cogwheel code [14], and ours, produced using Bilby. We believe that these merit further investigation, as Cogwheel uses a different approach to calculating the signal likelihood (relative binning) [59] compared to the one used in Bilby which is based on a method developed in [12], and it is

unclear from our investigations if this is the source of the difference, or if there is an additional difference we have not accounted for. Perhaps the most dramatic difference we observe is in the measurement of spin parameters by our approach and that employed by Cogwheel. A clearer understanding of how these differences arise would be a valuable future investigation.

The addition of 57 events to the 90 identified in GWTC-3 substantially increases the population of signals analysed using a GWTC-like analysis configuration, and the implications of these additional events to the understanding of compact binary populations also deserves future investigation.

With future developments in detector technology continually improving the sensitivity of the network of gravitational wave observatories we anticipate that the variety of search results from different groups and search pipelines will continue to grow, and so we present the use of Asimov as a means of creating consistent datasets for gravitational wave PE on public data.

6. Data availability

The data associated with this publication is available from Zenodo [60].

7. Acknowledgements

The authors wish to thank John Veitch and Christopher Berry for their suggestions throughout the production of these analyses and the associated missive, as well as various discussions with members of the Institute for Gravitational Research as we developed the analysis. We also thank Michael Williams for useful suggestions on the text, and the two anonymous reviewers for their insightful and thorough critique of the manuscript.

This research has made use of data or software obtained from the Gravitational Wave Open Science Center (gwosc.org), a service of the LIGO Scientific Collaboration, the Virgo Collaboration, and KAGRA. This material is based upon work supported by NSF's LIGO Laboratory which is a major facility fully funded by the National Science Foundation, as well as the Science and Technology Facilities Council (STFC) of the United Kingdom, the Max-Planck-Society (MPS), and the State of Niedersachsen/Germany for support of the construction of Advanced LIGO and construction and operation of the GEO600 detector. Additional support for Advanced LIGO was provided by the Australian Research Council. Virgo is funded, through the European Gravitational Observatory (EGO), by the French Centre National de Recherche Scientifique (CNRS), the Italian Istituto Nazionale di Fisica Nucleare (INFN) and the Dutch Nikhef, with contributions by institutions from Belgium, Germany, Greece, Hungary, Ireland, Japan, Monaco, Poland, Portugal, Spain. KAGRA is supported by Ministry of Education, Culture, Sports, Science and Technology (MEXT), Japan Society for the Promotion of Science (JSPS) in Japan; National Research

Foundation (NRF) and Ministry of Science and ICT (MSIT) in Korea; Academia Sinica (AS) and National Science and Technology Council (NSTC) in Taiwan.

DW is supported under STFC grant ST/V005634/1.

The analyses presented in this missive were run on the computing resources at the Institute for Gravitational Research at the University of Glasgow. We acknowledge the following software packages which were integral to this analysis: asimov [29], Bilby [13], Bilby_pipe [32], Bayeswave [31], PESummary [35], Dynesty [33], numpy [61], scipy[62], matplotlib[63], HTCondor [64], and astropy [44, 65, 66].

References

[1] B. P. Abbott et al. "Observation of Gravitational Waves from a Binary Black Hole Merger". In: *Physical Review Letters* 116.6 (Feb. 2016). ISSN: 1079-7114. DOI: 10.1103/physrevlett.116.061102. URL: http://dx.doi.org/10.1103/PhysRevLett.116.061102.

[2] B. P. Abbott et al. "GWTC-1: A Gravitational-Wave Transient Catalog of Compact Binary Mergers Observed by LIGO and Virgo during the First and Second Observing Runs". In: *Physical Review X* 9 (July 2019). Publisher: APS ADS Bibcode: 2019PhRvX...9c1040A, p. 031040. DOI: 10.1103/PhysRevX.9.031040. URL: https://ui.adsabs.harvard.edu/abs/2019PhRvX...9c1040A (visited on 08/14/2024).

[3] R. Abbott et al. "GWTC-2: Compact Binary Coalescences Observed by LIGO and Virgo during the First Half of the Third Observing Run". In: *Physical Review X* 11 (Apr. 2021). Publisher: APS ADS Bibcode: 2021PhRvX..11b1053A, p. 021053. DOI: 10.1103/PhysRevX.11.021053. URL: https://ui.adsabs.harvard.edu/abs/2021PhRvX..11b1053A (visited on 08/14/2024).

[4] R. Abbott et al. "GWTC-2.1: Deep extended catalog of compact binary coalescences observed by LIGO and Virgo during the first half of the third observing run". en. In: *Physical Review D* 109.2 (Jan. 2024). Version Number: 2, p. 022001. ISSN: 2470-0010, 2470-0029. DOI: 10.1103/PhysRevD.109.022001. URL: https://link.aps.org/doi/10.1103/PhysRevD.109.022001 (visited on 04/03/2025).

[5] R. Abbott et al. "GWTC-3: Compact Binary Coalescences Observed by LIGO and Virgo during the Second Part of the Third Observing Run". In: *Physical Review X* 13 (Oct. 2023). Publisher: APS ADS Bibcode: 2023PhRvX..13d1039A, p. 041039. DOI: 10.1103/PhysRevX.13.041039. URL: https://ui.adsabs.harvard.edu/abs/2023PhRvX..13d1039A (visited on 04/03/2025).

[6] Samantha A. Usman et al. "The PyCBC search for gravitational waves from compact binary coalescence". In: *Classical and Quantum Gravity* 33 (Nov. 2016), p. 215004. ISSN: 0264-9381. DOI: 10.1088/0264-9381/33/21/215004. URL:

https://ui.adsabs.harvard.edu/abs/2016CQGra..33u5004U (visited on 08/14/2024).

[7] T. Adams et al. "Low-latency analysis pipeline for compact binary coalescences in the advanced gravitational wave detector era". In: *Classical and Quantum Gravity* 33 (Sept. 2016). Publisher: IOP ADS Bibcode: 2016CQGra..33q5012A, p. 175012. ISSN: 0264-9381. DOI: 10.1088/0264-9381/33/17/175012. URL: https://ui.adsabs.harvard.edu/abs/2016CQGra..33q5012A (visited on 11/29/2024).

[8] Qi Chu et al. "SPIIR online coherent pipeline to search for gravitational waves from compact binary coalescences". In: *Physical Review D* 105.2 (Jan. 2022). Publisher: American Physical Society, p. 024023. DOI: 10.1103/PhysRevD.105.024023. URL: https://link.aps.org/doi/10.1103/PhysRevD.105.024023 (visited on 11/29/2024).

[9] S. Klimenko et al. "Method for detection and reconstruction of gravitational wave transients with networks of advanced detectors". In: *Physical Review D* 93 (Feb. 2016). Publisher: APS ADS Bibcode: 2016PhRvD..93d2004K, p. 042004. ISSN: 1550-79980556-2821. DOI: 10.1103/PhysRevD.93.042004. URL: https://ui.adsabs.harvard.edu/abs/2016PhRvD..93d2004K (visited on 11/29/2024).

[10] Will M. Farr et al. "Counting and confusion: Bayesian rate estimation with multiple populations". In: *Physical Review D* 91.2 (Jan. 2015). Publisher: American Physical Society, p. 023005. DOI: 10.1103/PhysRevD.91.023005. URL: https://link.aps.org/doi/10.1103/PhysRevD.91.023005 (visited on 12/01/2024).

[11] F. Guglielmetti, R. Fischer, and V. Dose. "Background–source separation in astronomical images with Bayesian probability theory – I. The method". In: *Monthly Notices of the Royal Astronomical Society* 396.1 (June 2009), pp. 165–190. ISSN: 0035-8711. DOI: 10.1111/j.1365-2966.2009.14739.x. URL: https://doi.org/10.1111/j.1365-2966.2009.14739.x (visited on 12/01/2024).

[12] J. Veitch et al. "Parameter estimation for compact binaries with ground-based gravitational-wave observations using the LALInference software library". In: *Physical Review D* 91 (Feb. 2015). Publisher: APS ADS Bibcode: 2015PhRvD..91d2003V, p. 042003. ISSN: 1550-79980556-2821. DOI: 10.1103/PhysRevD.91.042003. URL: https://ui.adsabs.harvard.edu/abs/2015PhRvD..91d2003V (visited on 11/29/2024).

[13] Gregory Ashton et al. "Bilby: A User-friendly Bayesian Inference Library for Gravitational-wave Astronomy". In: *The Astrophysical Journal Supplement Series* 241.2 (Apr. 2019), p. 27. ISSN: 1538-4365. DOI: 10.3847/1538-4365/ab06fc. URL: http://dx.doi.org/10.3847/1538-4365/ab06fc.

[14] Javier Roulet et al. "Fast marginalization algorithm for optimizing gravitational wave detection, parameter estimation, and sky localization". In: *Physical Review D* 110 (Aug. 2024). Publisher: APS ADS Bibcode: 2024PhRvD.110d4010R, p. 044010. ISSN: 1550-79980556-2821. DOI: 10.1103/PhysRevD.110.044010.

URL: https://ui.adsabs.harvard.edu/abs/2024PhRvD.110d4010R (visited on 11/19/2024).

[15] Hunter Gabbard et al. "Bayesian parameter estimation using conditional variational autoencoders for gravitational-wave astronomy". In: *Nature Physics* 18.1 (Jan. 2022), pp. 112–117. DOI: 10.1038/s41567-021-01425-7. arXiv: 1909.06296 [astro-ph.IM].

[16] Maximilian Dax et al. "Real-Time Gravitational Wave Science with Neural Posterior Estimation". In: *Physical Review Letters* 127.24, 241103 (Dec. 2021), p. 241103. DOI: 10.1103/PhysRevLett.127.241103. arXiv: 2106.12594 [gr-qc].

[17] Alexander H. Nitz et al. "1-OGC: The First Open Gravitational-wave Catalog of Binary Mergers from Analysis of Public Advanced LIGO Data". In: *The Astrophysical Journal* 872.2, 195 (Feb. 2019), p. 195. DOI: 10.3847/1538-4357/ab0108. arXiv: 1811.01921 [gr-qc].

[18] Alexander H. Nitz et al. "2-OGC: Open Gravitational-wave Catalog of Binary Mergers from Analysis of Public Advanced LIGO and Virgo Data". In: *The Astrophysical Journal* 891.2, 123 (Mar. 2020), p. 123. DOI: 10.3847/1538-4357/ab733f. arXiv: 1910.05331 [astro-ph.HE].

[19] Alexander H. Nitz et al. "3-OGC: Catalog of Gravitational Waves from Compact-binary Mergers". In: *The Astrophysical Journal* 922.1, 76 (Nov. 2021), p. 76. DOI: 10.3847/1538-4357/ac1c03. arXiv: 2105.09151 [astro-ph.HE].

[20] Alexander H. Nitz et al. "4-OGC: Catalog of Gravitational Waves from Compact Binary Mergers". In: *The Astrophysical Journal* 946.2, 59 (Apr. 2023), p. 59. DOI: 10.3847/1538-4357/aca591.

[21] Tejaswi Venumadhav et al. "New search pipeline for compact binary mergers: Results for binary black holes in the first observing run of Advanced LIGO". In: *Physical Review D* 100 (July 2019). Publisher: APS ADS Bibcode: 2019PhRvD.100b3011V, p. 023011. ISSN: 1550-79980556-2821. DOI: 10.1103/PhysRevD.100.023011. URL: https://ui.adsabs.harvard.edu/abs/2019PhRvD.100b3011V (visited on 08/14/2024).

[22] Tejaswi Venumadhav et al. "New binary black hole mergers in the second observing run of Advanced LIGO and Advanced Virgo". In: *Physical Review D* 101 (Apr. 2020). Publisher: APS ADS Bibcode: 2020PhRvD.101h3030V, p. 083030. ISSN: 1550-79980556-2821. DOI: 10.1103/PhysRevD.101.083030. URL: https://ui.adsabs.harvard.edu/abs/2020PhRvD.101h3030V (visited on 08/14/2024).

[23] Seth Olsen et al. "New binary black hole mergers in the LIGO-Virgo O3a data". In: *Physical Review D* 106 (Aug. 2022). Publisher: APS ADS Bibcode: 2022PhRvD.106d3009O, p. 043009. ISSN: 1550-79980556-2821. DOI: 10.1103/PhysRevD.106.043009. URL: https://ui.adsabs.harvard.edu/abs/2022PhRvD.106d3009O (visited on 08/14/2024).

[24] Ajit Kumar Mehta et al. "New binary black hole mergers in the LIGO-Virgo O3b data". In: *Physical Review D* 111 (Jan. 2025). Publication Title: arXiv e-prints Publisher: APS ADS Bibcode: 2025PhRvD.111b4049M ADS Bibcode: 2023arXiv231106061M, p. 024049. ISSN: 1550-79980556-2821. DOI: 10.1103/PhysRevD.111.024049. URL: https://ui.adsabs.harvard.edu/abs/2025PhRvD.111b4049M (visited on 04/03/2025).

[25] Digvijay Wadekar et al. *New black hole mergers in the LIGO-Virgo O3 data from a gravitational wave search including higher-order harmonics*. Publication Title: arXiv e-prints ADS Bibcode: 2023arXiv231206631W. Dec. 2023. DOI: 10.48550/arXiv.2312.06631. URL: https://ui.adsabs.harvard.edu/abs/2023arXiv231206631W (visited on 08/14/2024).

[26] Praveen Kumar and Thomas Dent. "Optimized search for a binary black hole merger population in LIGO-Virgo O3 data". In: *Physical Review D* 110.4, 043036 (Aug. 2024), p. 043036. DOI: 10.1103/PhysRevD.110.043036. arXiv: 2403.10439 [gr-qc].

[27] T. Mishra et al. "Gravitational waves detected by a burst search in LIGO/Virgo's third observing run". In: *Physical Review D* 111 (Jan. 2025). Publication Title: arXiv e-prints Publisher: APS ADS Bibcode: 2025PhRvD.111b3054M ADS Bibcode: 2024arXiv241015191M, p. 023054. ISSN: 1550-79980556-2821. DOI: 10.1103/PhysRevD.111.023054. URL: https://ui.adsabs.harvard.edu/abs/2025PhRvD.111b3054M (visited on 04/03/2025).

[28] Alexandra E. Koloniari et al. "New gravitational wave discoveries enabled by machine learning". In: *Machine Learning: Science and Technology* 6 (Mar. 2025). Publisher: IOP ADS Bibcode: 2025MLS&T...6a5054K, p. 015054. DOI: 10.1088/2632-2153/adb5ed. URL: https://ui.adsabs.harvard.edu/abs/2025MLS&T...6a5054K (visited on 04/03/2025).

[29] Daniel Williams et al. "Asimov: A framework for coordinating parameter estimation workflows". en. In: *Journal of Open Source Software* 8.84 (Apr. 2023), p. 4170. ISSN: 2475-9066. DOI: 10.21105/joss.04170. URL: https://joss.theoj.org/papers/10.21105/joss.04170 (visited on 11/29/2024).

[30] Cameron Mills and Stephen Fairhurst. "Measuring gravitational-wave higher-order multipoles". In: *Physical Review D* 103 (Jan. 2021). Publisher: APS ADS Bibcode: 2021PhRvD.103b4042M, p. 024042. ISSN: 1550-79980556-2821. DOI: 10.1103/PhysRevD.103.024042. URL: https://ui.adsabs.harvard.edu/abs/2021PhRvD.103b4042M (visited on 03/14/2025).

[31] Neil J Cornish and Tyson B Littenberg. "Bayeswave: Bayesian inference for gravitational wave bursts and instrument glitches". In: *Classical and Quantum Gravity* 32.13 (June 2015), p. 135012. ISSN: 1361-6382. DOI: 10.1088/0264-9381/32/13/135012. URL: http://dx.doi.org/10.1088/0264-9381/32/13/135012.

[32] I M Romero-Shaw et al. "Bayesian inference for compact binary coalescences with bilby: validation and application to the first LIGO–Virgo gravitational-wave transient catalogue". In: *Monthly Notices of the Royal Astronomical Society* 499.3 (Sept. 2020), pp. 3295–3319. ISSN: 1365-2966. DOI: 10.1093/mnras/staa2850. URL: http://dx.doi.org/10.1093/mnras/staa2850.

[33] Joshua S. Speagle. "DYNESTY: a dynamic nested sampling package for estimating Bayesian posteriors and evidences". In: *Monthly Notices of the Royal Astronomical Society* 493.3 (Apr. 2020), pp. 3132–3158. DOI: 10.1093/mnras/staa278. arXiv: 1904.02180 [astro-ph.IM].

[34] Geraint Pratten et al. "Computationally efficient models for the dominant and subdominant harmonic modes of precessing binary black holes". In: *Physical Review D* 103.10 (May 2021). ISSN: 2470-0029. DOI: 10.1103/physrevd.103.104056. URL: http://dx.doi.org/10.1103/PhysRevD.103.104056.

[35] Charlie Hoy and Vivien Raymond. "PESummary: the code agnostic Parameter Estimation Summary page builder". In: *SoftwareX* 15 (2021), p. 100765. DOI: 10.1016/j.softx.2021.100765. arXiv: 2006.06639 [astro-ph.IM].

[36] Colm Talbot et al. *bilby-dev/bilby: v2.1.1*. Nov. 2024. URL: https://doi.org/10.5281/zenodo.14025640.

[37] Héctor Estellés Estrella, Serguei Ossokine, and Daniel Williams. *pe-configurator*. Version 1.0.1. Nov. 2023. DOI: 10.5281/zenodo.10133300. URL: https://doi.org/10.5281/zenodo.10133300.

[38] Serguei Ossokine et al. "Multipolar effective-one-body waveforms for precessing binary black holes: Construction and validation". In: *Physical Review D* 102.4 (Aug. 2020). ISSN: 2470-0029. DOI: 10.1103/physrevd.102.044055. URL: http://dx.doi.org/10.1103/PhysRevD.102.044055.

[39] C. Pankow et al. "Novel scheme for rapid parallel parameter estimation of gravitational waves from compact binary coalescences". In: *Physical Review D* 92.2 (July 2015). Publisher: American Physical Society, p. 023002. DOI: 10.1103/PhysRevD.92.023002. URL: https://link.aps.org/doi/10.1103/PhysRevD.92.023002 (visited on 04/03/2025).

[40] Richard O'Shaughnessy, Jonathan Blackman, and Scott E. Field. "An architecture for efficient gravitational wave parameter estimation with multimodal linear surrogate models". en. In: *Classical and Quantum Gravity* 34.14 (June 2017). Publisher: IOP Publishing, p. 144002. ISSN: 0264-9381. DOI: 10.1088/1361-6382/aa7649. URL: https://dx.doi.org/10.1088/1361-6382/aa7649 (visited on 09/10/2024).

[41] J. Lange et al. "Parameter estimation method that directly compares gravitational wave observations to numerical relativity". In: *Physical Review D* 96.10 (Nov. 2017). Publisher: American Physical Society, p. 104041. DOI: 10.1103/PhysRevD.96.104041. URL: https://link.aps.org/doi/10.1103/PhysRevD.96.104041 (visited on 04/03/2025).

[42] D. Wysocki et al. "Accelerating parameter inference with graphics processing units". In: *Physical Review D* 99.8 (Apr. 2019). Publisher: American Physical Society, p. 084026. DOI: 10.1103/PhysRevD.99.084026. URL: https://link.aps.org/doi/10.1103/PhysRevD.99.084026 (visited on 04/03/2025).

[43] D. Fernando, R. O'Shaughnessy, and D. Williams. *Efficient reanalysis of events from GWTC-3 with RIFT and asimov*. arXiv:2412.02999 [astro-ph]. Dec. 2024. DOI: 10.48550/arXiv.2412.02999. URL: http://arxiv.org/abs/2412.02999 (visited on 12/05/2024).

[44] The Astropy Collaboration et al. "The Astropy Project: Sustaining and Growing a Community-oriented Open-source Project and the Latest Major Release (v5.0) of the Core Package". In: *The Astrophysical Journal* 935.2 (Aug. 2022). arXiv:2206.14220 [astro-ph], p. 167. ISSN: 0004-637X, 1538-4357. DOI: 10.3847/1538-4357/ac7c74. URL: http://arxiv.org/abs/2206.14220 (visited on 12/11/2024).

[45] P. a. R. Ade et al. "Planck 2015 results - XIII. Cosmological parameters". en. In: *Astronomy & Astrophysics* 594 (Oct. 2016). Publisher: EDP Sciences, A13. ISSN: 0004-6361, 1432-0746. DOI: 10.1051/0004-6361/201525830. URL: https://www.aanda.org/articles/aa/abs/2016/10/aa25830-15/aa25830-15.html (visited on 12/11/2024).

[46] S. Kullback and R. A. Leibler. "On Information and Sufficiency". In: *The Annals of Mathematical Statistics* 22.1 (Mar. 1951). Publisher: Institute of Mathematical Statistics, pp. 79–86. ISSN: 0003-4851, 2168-8990. DOI: 10.1214/aoms/1177729694. URL: https://projecteuclid.org/journals/annals-of-mathematical-statistics/volume-22/issue-1/On-Information-and-Sufficiency/10.1214/aoms/1177729694.full (visited on 03/17/2025).

[47] Barak Zackay et al. "Highly spinning and aligned binary black hole merger in the Advanced LIGO first observing run". In: *Physical Review D* 100.2, 023007 (July 2019), p. 023007. DOI: 10.1103/PhysRevD.100.023007. arXiv: 1902.10331 [astro-ph.HE].

[48] Yiwen Huang et al. "Source properties of the lowest signal-to-noise-ratio binary black hole detections". In: *Physical Review D* 102.10, 103024 (Nov. 2020), p. 103024. DOI: 10.1103/PhysRevD.102.103024. arXiv: 2003.04513 [gr-qc].

[49] Gregory Ashton and Eric Thrane. "The astrophysical odds of GW151216". In: *Monthly Notices of the Royal Astronomical Society* 498.2 (Oct. 2020), pp. 1905–1910. DOI: 10.1093/mnras/staa2332. arXiv: 2006.05039 [astro-ph.HE].

[50] Shreejit Jadhav et al. "Improving significance of binary black hole mergers in Advanced LIGO data using deep learning: Confirmation of GW151216". In: *Physical Review D* 104.6, 064051 (Sept. 2021), p. 064051. DOI: 10.1103/PhysRevD.104.064051. arXiv: 2010.08584 [gr-qc].

[51] Sebastian Khan et al. "Frequency-domain gravitational waves from nonprecessing black-hole binaries. II. A phenomenological model for the advanced detector era". In: *Physical Review D* 93 (Feb. 2016). Publisher: APS ADS Bibcode: 2016PhRvD..93d4007K, p. 044007. ISSN: 1550-79980556-2821. DOI: 10.1103/PhysRevD.93.044007. URL: https://ui.adsabs.harvard.edu/abs/2016PhRvD..93d4007K (visited on 12/09/2024).

[52] Sascha Husa et al. "Frequency-domain gravitational waves from nonprecessing black-hole binaries. I. New numerical waveforms and anatomy of the signal". In: *Physical Review D* 93 (Feb. 2016). Publisher: APS ADS Bibcode: 2016PhRvD..93d4006H, p. 044006. ISSN: 1550-79980556-2821. DOI: 10.1103/PhysRevD.93.044006. URL: https://ui.adsabs.harvard.edu/abs/2016PhRvD..93d4006H (visited on 12/09/2024).

[53] The LIGO Scientific Collaboration et al. "Open data from the first and second observing runs of Advanced LIGO and Advanced Virgo". In: *SoftwareX* 13 (Jan. 2021). arXiv:1912.11716 [gr-qc], p. 100658. ISSN: 23527110. DOI: 10.1016/j.softx.2021.100658. URL: http://arxiv.org/abs/1912.11716 (visited on 03/21/2025).

[54] Hang Yu et al. "Accurate and efficient waveform model for precessing binary black holes". In: *Physical Review D* 108 (Sept. 2023). Publisher: APS ADS Bibcode: 2023PhRvD.108f4059Y, p. 064059. ISSN: 1550-79980556-2821. DOI: 10.1103/PhysRevD.108.064059. URL: https://ui.adsabs.harvard.edu/abs/2023PhRvD.108f4059Y (visited on 12/09/2024).

[55] Carl L. Rodriguez et al. "Illuminating Black Hole Binary Formation Channels with Spins in Advanced Ligo". en. In: *The Astrophysical Journal Letters* 832.1 (Nov. 2016), p. L2. ISSN: 2041-8205. DOI: 10.3847/2041-8205/832/1/L2. URL: https://dx.doi.org/10.3847/2041-8205/832/1/L2 (visited on 04/01/2025).

[56] Gregory Ashton et al. "Parameterised population models of transient non-Gaussian noise in the LIGO gravitational-wave detectors". In: *Classical and Quantum Gravity* 39.17 (Sept. 2022). arXiv:2110.02689 [gr-qc], p. 175004. ISSN: 0264-9381, 1361-6382. DOI: 10.1088/1361-6382/ac8094. URL: http://arxiv.org/abs/2110.02689 (visited on 04/01/2025).

[57] Gregory Ashton, Eric Thrane, and Rory J. E. Smith. "Gravitational wave detection without boot straps: A Bayesian approach". In: *Physical Review D* 100 (Dec. 2019). Publisher: APS ADS Bibcode: 2019PhRvD.100l3018A, p. 123018. ISSN: 1550-79980556-2821. DOI: 10.1103/PhysRevD.100.123018. URL: https://ui.adsabs.harvard.edu/abs/2019PhRvD.100l3018A (visited on 12/08/2024).

[58] Gregory Ashton and Eric Thrane. "The astrophysical odds of GW151216". In: *Monthly Notices of the Royal Astronomical Society* 498 (Oct. 2020). Publisher: OUP ADS Bibcode: 2020MNRAS.498.1905A, pp. 1905–1910. ISSN: 0035-8711. DOI: 10.1093/mnras/staa2332. URL: https://ui.adsabs.harvard.edu/abs/2020MNRAS.498.1905A (visited on 12/08/2024).

[59] Javier Roulet et al. "Removing degeneracy and multimodality in gravitational wave source parameters". In: *Physical Review D* 106 (Dec. 2022). Publisher: APS ADS Bibcode: 2022PhRvD.106l3015R, p. 123015. ISSN: 1550-79980556-2821. DOI: 10.1103/PhysRevD.106.123015. URL: https://ui.adsabs.harvard.edu/abs/2022PhRvD.106l3015R (visited on 12/12/2024).

[60] Daniel Williams. *Beyond GWTC-3: Analysing and verifying new gravitational-wave events from the 4-OGC Catalogue*. Version 2. Zenodo, Jan. 2025. DOI: 10.5281/zenodo.10479523. URL: https://doi.org/10.5281/zenodo.10479523.

[61] Charles R. Harris et al. "Array programming with NumPy". en. In: *Nature* 585.7825 (Sept. 2020). Publisher: Nature Publishing Group, pp. 357–362. ISSN: 1476-4687. DOI: 10.1038/s41586-020-2649-2. URL: https://www.nature.com/articles/s41586-020-2649-2 (visited on 12/10/2024).

[62] Pauli Virtanen et al. "SciPy 1.0: fundamental algorithms for scientific computing in Python". In: *Nature Methods* 17 (Feb. 2020). ADS Bibcode: 2020NatMe..17..261V, pp. 261–272. DOI: 10.1038/s41592-019-0686-2. URL: https://ui.adsabs.harvard.edu/abs/2020NatMe..17..261V (visited on 12/01/2024).

[63] John D. Hunter. "Matplotlib: A 2D Graphics Environment". In: *Computing in Science and Engineering* 9 (May 2007). ADS Bibcode: 2007CSE.....9...90H, pp. 90–95. DOI: 10.1109/MCSE.2007.55. URL: https://ui.adsabs.harvard.edu/abs/2007CSE.....9...90H (visited on 12/01/2024).

[64] Douglas Thain, Todd Tannenbaum, and Miron Livny. "Distributed computing in practice: the Condor experience". en. In: *Concurrency and Computation: Practice and Experience* 17.2-4 (2005). _eprint: https://onlinelibrary.wiley.com/doi/pdf/10.1002/cpe.938, pp. 323–356. ISSN: 1532-0634. DOI: 10.1002/cpe.938. URL: https://onlinelibrary.wiley.com/doi/abs/10.1002/cpe.938 (visited on 12/01/2024).

[65] Astropy Collaboration et al. "Astropy: A community Python package for astronomy". In: *Astronomy and Astrophysics* 558 (Oct. 2013). ADS Bibcode: 2013A&A...558A..33A, A33. ISSN: 0004-6361. DOI: 10.1051/0004-6361/201322068. URL: https://ui.adsabs.harvard.edu/abs/2013A&A...558A..33A (visited on 12/11/2024).

[66] Astropy Collaboration et al. "The Astropy Project: Building an Open-science Project and Status of the v2.0 Core Package". In: *The Astronomical Journal* 156 (Sept. 2018). Publisher: IOP ADS Bibcode: 2018AJ....156..123A, p. 123. ISSN: 0004-6256. DOI: 10.3847/1538-3881/aabc4f. URL: https://ui.adsabs.harvard.edu/abs/2018AJ....156..123A (visited on 12/11/2024).

[67] *Asimov documentation*. URL: https://asimov.docs.ligo.org/asimov/master/index.html (visited on 12/10/2024).

Event	$M_{\rm src}/{\rm M}_\odot$	$\mathcal{M}_{\rm src}/{\rm M}_\odot$	$m_{1,\rm src}/{\rm M}_\odot$	$m_{2,\rm src}/{\rm M}_\odot$	$\chi_{\rm eff}$	$D_{\rm L}/{\rm Mpc}$	z
GW 151205_195525	$104.9^{+26.2}_{-25.2}$	$43.6^{+12.1}_{-11.4}$	$63.3^{+21.5}_{-19.6}$	$41.6^{+17.4}_{-17.7}$	$0.13^{+0.40}_{-0.36}$	3390^{+2510}_{-2190}	$0.6^{+0.3}_{-0.3}$
GW 151216_092416	$53.9^{+11.1}_{-11.8}$	$20.7^{+3.9}_{-5.0}$	$37.6^{+12.0}_{-12.5}$	$15.8^{+6.9}_{-6.5}$	$0.54^{+0.28}_{-0.36}$	1950^{+1090}_{-1070}	$0.4^{+0.2}_{-0.2}$
GW 170121_212536	$57.3^{+7.7}_{-7.6}$	$24.5^{+3.3}_{-3.2}$	$32.3^{+7.5}_{-6.4}$	$24.6^{+5.4}_{-5.7}$	$-0.25^{+0.26}_{-0.27}$	1060^{+890}_{-710}	$0.2^{+0.2}_{-0.1}$
GW 170202_135657	$43.5^{+8.8}_{-8.4}$	$18.0^{+3.2}_{-3.3}$	$26.4^{+9.6}_{-8.0}$	$16.7^{+5.9}_{-5.5}$	$-0.11^{+0.32}_{-0.31}$	1470^{+900}_{-830}	$0.3^{+0.1}_{-0.1}$
GW 170304_163753	$76.0^{+14.9}_{-13.1}$	$32.2^{+6.8}_{-5.9}$	$44.1^{+11.8}_{-10.4}$	$31.9^{+10.0}_{-10.0}$	$0.13^{+0.27}_{-0.26}$	2590^{+1550}_{-1570}	$0.5^{+0.2}_{-0.2}$
GW 170403_230611	$82.3^{+17.6}_{-15.2}$	$34.9^{+7.8}_{-6.9}$	$47.4^{+14.1}_{-11.9}$	$34.9^{+11.0}_{-11.0}$	$-0.24^{+0.33}_{-0.34}$	3180^{+2000}_{-1930}	$0.5^{+0.3}_{-0.3}$
GW 170425_055334	$76.8^{+17.4}_{-15.4}$	$31.5^{+7.1}_{-6.4}$	$48.3^{+16.5}_{-15.2}$	$28.5^{+10.3}_{-10.7}$	$-0.05^{+0.28}_{-0.31}$	2430^{+1700}_{-1430}	$0.4^{+0.2}_{-0.2}$
GW 170727_010430	$70.4^{+11.7}_{-10.6}$	$30.1^{+5.2}_{-4.6}$	$39.8^{+9.4}_{-8.3}$	$30.4^{+7.8}_{-7.8}$	$-0.04^{+0.25}_{-0.27}$	2450^{+1410}_{-1380}	$0.4^{+0.2}_{-0.2}$
GW 190426_082124	$68.7^{+20.5}_{-18.2}$	$28.9^{+8.7}_{-7.4}$	$40.6^{+16.0}_{-13.8}$	$27.7^{+10.8}_{-10.6}$	$-0.13^{+0.31}_{-0.35}$	4920^{+3530}_{-3080}	$0.8^{+0.4}_{-0.4}$
GW 190427_180650	$18.0^{+2.7}_{-2.3}$	$7.3^{+0.6}_{-0.6}$	$11.6^{+3.9}_{-3.5}$	$6.3^{+1.9}_{-1.7}$	$0.00^{+0.18}_{-0.13}$	1000^{+540}_{-520}	$0.2^{+0.1}_{-0.1}$

Table A1. The median, and 90% highest probability density intervals (that is, the narrowest region containing 90% of the posterior probability) for the selected inferred source properties of the signals from O1 and O2 analysed in this work. The columns show the total mass of the binary $M_{\rm src}$; the chirp mass $\mathcal{M}_{\rm src}$; the component objects' masses $m_{1,\rm src}$, and $m_{2,\rm src}$; the effective inspiral spin; $\chi_{\rm eff}$; the luminosity distance $D_{\rm L}$; and the redshift z. All masses are quoted in the source frame, and are derived from inference using the IMRPhenomXPHM BBH waveform model.

Appendix A. Source properties – tables

In this section we present the source properties and their associated uncertainties for the events from O1 and O2 (table A1) and O3 (table A2).

Appendix B. Asimov blueprints

This section provides a short technical overview of Asimov's "blueprint" files which are used to configure analyses in a consistent way across different analysis pipelines and computing facilities while abstracting as much of that configuration as possible. Blueprints are intended to provide a uniform configuration interface for a number of different analysis codes, allowing consistent and comparable analyses to be performed in a straightforward manner. In this work we perform parameter estimation (PE) analyses only using the Bilby PE library, but within our workflow we also ran a Bayeswave analysis; Asimov blueprints allow this workflow to be specified with minimal repetition or reconfiguration between events. Asimov also makes it possible to replace parts of the workflow with minimal additional work, for example the Bilby analyses could be replaced by a LALInference [12] or RIFT [39–41, 43] analysis by changing a single line in a blueprint, where previously the various configuration parameters would need to be mapped between the Bilby and other code's input format.

To achieve this, it is normal to configure an Asimov *project* with a series of different settings; these are then treated hierarchically by Asimov when constructing an analysis, with settings specified with higher precedence over-riding those from below. This allows almost total flexibility when creating an individual analysis, while generally ensuring consistency. In sequence of increasing precedence these are:

Event	$M/\mathrm{M}_\odot$	$\mathcal{M}/\mathrm{M}_\odot$	$m_1/\mathrm{M}_\odot$	$m_2/\mathrm{M}_\odot$	$\chi_{\rm eff}$	$D_\mathrm{L}/\mathrm{Mpc}$	z
GW 190511_125545	$66.4^{+21.5}_{-17.0}$	$27.2^{+9.7}_{-7.6}$	$41.9^{+15.8}_{-14.1}$	$25.1^{+12.6}_{-12.4}$	$0.23^{+0.29}_{-0.29}$	3090^{+2420}_{-2000}	$0.5^{+0.3}_{-0.3}$
GW 190511_163209	$116.2^{+116.5}_{-77.5}$	$39.2^{+35.5}_{-23.6}$	$87.2^{+109.4}_{-65.8}$	$24.7^{+26.7}_{-16.7}$	$0.01^{+0.49}_{-0.40}$	4800^{+8910}_{-4440}	$0.8^{+1.0}_{-0.6}$
GW 190514_065416	$68.2^{+16.8}_{-13.5}$	$28.9^{+6.8}_{-5.7}$	$39.4^{+13.8}_{-10.8}$	$28.7^{+9.0}_{-9.1}$	$-0.17^{+0.29}_{-0.32}$	4080^{+2370}_{-2280}	$0.7^{+0.3}_{-0.3}$
GW 190523_085933	$64.0^{+34.5}_{-34.5}$	$23.2^{+18.0}_{-12.0}$	$46.2^{+24.6}_{-27.0}$	$16.9^{+24.9}_{-11.6}$	$0.40^{+0.35}_{-0.46}$	4580^{+3870}_{-3050}	$0.7^{+0.5}_{-0.4}$
GW 190524_134109	$113.1^{+34.7}_{-29.3}$	$46.0^{+16.8}_{-13.8}$	$70.0^{+27.5}_{-23.8}$	$43.6^{+22.1}_{-24.4}$	$0.27^{+0.37}_{-0.39}$	7340^{+5150}_{-4680}	$1.1^{+0.6}_{-0.6}$
GW 190530_030659	$52.4^{+10.8}_{-10.2}$	$21.4^{+3.7}_{-3.7}$	$32.1^{+13.8}_{-10.2}$	$19.4^{+6.7}_{-7.3}$	$0.36^{+0.22}_{-0.23}$	2830^{+1620}_{-1580}	$0.5^{+0.2}_{-0.2}$
GW 190530_133833	$145.8^{+55.8}_{-48.6}$	$58.6^{+23.6}_{-20.6}$	$92.7^{+45.5}_{-39.3}$	$51.9^{+29.2}_{-29.6}$	$0.05^{+0.44}_{-0.43}$	6810^{+6070}_{-5040}	$1.0^{+0.7}_{-0.6}$
GW 190604_103812	$154.0^{+81.0}_{-74.7}$	$55.4^{+31.5}_{-25.5}$	$114.1^{+69.2}_{-70.1}$	$40.1^{+29.7}_{-25.8}$	$0.54^{+0.33}_{-0.61}$	7730^{+6320}_{-5470}	$1.1^{+0.7}_{-0.7}$
GW 190605_025957	$214.8^{+104.6}_{-89.3}$	$88.1^{+45.0}_{-41.2}$	$132.4^{+81.2}_{-60.6}$	$83.3^{+53.5}_{-60.2}$	$0.10^{+0.45}_{-0.38}$	5290^{+4880}_{-4310}	$0.8^{+0.6}_{-0.6}$
GW 190607_083827	$74.3^{+16.6}_{-14.7}$	$31.6^{+7.4}_{-6.6}$	$42.6^{+11.8}_{-10.3}$	$31.8^{+10.1}_{-10.1}$	$-0.00^{+0.29}_{-0.30}$	4010^{+2540}_{-2300}	$0.7^{+0.3}_{-0.3}$
GW 190614_134749	$64.3^{+24.3}_{-19.0}$	$26.3^{+9.6}_{-7.6}$	$40.3^{+20.6}_{-15.2}$	$24.0^{+11.2}_{-11.4}$	$-0.00^{+0.31}_{-0.32}$	4140^{+3140}_{-2730}	$0.7^{+0.4}_{-0.4}$
GW 190615_030234	$118.0^{+25.8}_{-23.1}$	$49.8^{+12.5}_{-10.9}$	$68.9^{+18.1}_{-16.8}$	$49.8^{+18.4}_{-18.9}$	$0.00^{+0.31}_{-0.31}$	4540^{+2650}_{-2480}	$0.7^{+0.3}_{-0.3}$
GW 190705_164632	$83.9^{+25.1}_{-23.9}$	$33.6^{+11.2}_{-10.3}$	$53.8^{+20.8}_{-20.0}$	$29.4^{+15.3}_{-14.7}$	$0.26^{+0.31}_{-0.32}$	3610^{+3560}_{-2670}	$0.6^{+0.5}_{-0.4}$
GW 190707_083226	$87.3^{+20.1}_{-18.0}$	$35.9^{+8.9}_{-7.9}$	$53.5^{+18.4}_{-15.9}$	$33.3^{+13.3}_{-13.9}$	$-0.05^{+0.31}_{-0.34}$	3660^{+2740}_{-2330}	$0.6^{+0.4}_{-0.3}$
GW 190711_030756	$85.3^{+33.9}_{-22.6}$	$31.1^{+6.7}_{-6.4}$	$62.8^{+39.6}_{-25.5}$	$21.5^{+9.9}_{-9.8}$	$0.05^{+0.38}_{-0.28}$	2260^{+1520}_{-1320}	$0.4^{+0.2}_{-0.2}$
GW 190718_160159	$16.9^{+2.6}_{-2.3}$	$7.0^{+0.7}_{-0.7}$	$9.9^{+4.6}_{-2.5}$	$6.7^{+1.8}_{-2.3}$	$0.61^{+0.21}_{-0.47}$	1370^{+670}_{-660}	$0.3^{+0.1}_{-0.1}$
GW 190725_174728	$18.2^{+2.5}_{-2.1}$	$7.5^{+0.5}_{-0.5}$	$11.6^{+3.6}_{-3.3}$	$6.4^{+1.9}_{-1.5}$	$-0.05^{+0.17}_{-0.14}$	1020^{+460}_{-460}	$0.2^{+0.1}_{-0.1}$
GW 190805_105432	$21.7^{+3.1}_{-2.9}$	$8.8^{+0.8}_{-0.8}$	$14.2^{+4.0}_{-4.2}$	$7.4^{+2.1}_{-1.8}$	$-0.10^{+0.16}_{-0.16}$	1440^{+680}_{-690}	$0.3^{+0.1}_{-0.1}$
GW 190806_033721	$110.5^{+31.8}_{-29.2}$	$42.4^{+15.2}_{-12.8}$	$74.3^{+29.7}_{-28.5}$	$35.1^{+21.6}_{-20.0}$	$0.52^{+0.29}_{-0.39}$	8120^{+5970}_{-5110}	$1.2^{+0.7}_{-0.6}$
GW 190814_192009	$120.8^{+36.5}_{-30.4}$	$50.3^{+17.2}_{-13.9}$	$72.9^{+25.2}_{-23.2}$	$48.5^{+23.0}_{-22.6}$	$0.19^{+0.38}_{-0.37}$	7290^{+5130}_{-4700}	$1.1^{+0.6}_{-0.6}$
GW 190818_232544	$110.7^{+37.2}_{-34.9}$	$41.0^{+15.0}_{-13.5}$	$78.1^{+37.8}_{-34.9}$	$30.7^{+21.3}_{-17.6}$	$0.41^{+0.32}_{-0.45}$	4570^{+3980}_{-3150}	$0.7^{+0.5}_{-0.4}$
GW 190821_124821	$14.0^{+2.8}_{-2.8}$	$4.8^{+0.3}_{-0.2}$	$10.9^{+3.5}_{-3.8}$	$3.0^{+1.1}_{-0.7}$	$-0.16^{+0.23}_{-0.31}$	800^{+310}_{-350}	$0.2^{+0.1}_{-0.1}$
GW 190904_104631	$63.8^{+39.7}_{-37.3}$	$26.1^{+15.8}_{-15.3}$	$39.7^{+31.4}_{-26.8}$	$23.6^{+16.9}_{-16.3}$	$0.00^{+0.33}_{-0.34}$	4580^{+4620}_{-3210}	$0.7^{+0.6}_{-0.4}$
GW 190906_054335	$62.6^{+19.4}_{-17.0}$	$25.7^{+8.4}_{-8.0}$	$39.1^{+15.6}_{-13.6}$	$23.8^{+11.0}_{-12.1}$	$0.09^{+0.35}_{-0.32}$	4900^{+3620}_{-3140}	$0.8^{+0.5}_{-0.4}$
GW 190910_012619	$38.5^{+5.0}_{-4.9}$	$9.6^{+0.8}_{-0.9}$	$34.3^{+5.1}_{-5.2}$	$4.2^{+0.7}_{-0.6}$	$-0.55^{+0.20}_{-0.22}$	990^{+550}_{-530}	$0.2^{+0.1}_{-0.1}$
GW 190911_195101	$142.1^{+42.9}_{-34.1}$	$59.4^{+19.2}_{-15.7}$	$84.5^{+30.8}_{-26.6}$	$58.3^{+25.3}_{-26.0}$	$0.11^{+0.41}_{-0.38}$	6940^{+4380}_{-4440}	$1.0^{+0.5}_{-0.5}$
GW 190916_200658	$69.6^{+17.6}_{-15.8}$	$27.6^{+7.5}_{-6.5}$	$45.0^{+18.7}_{-15.2}$	$23.8^{+11.8}_{-11.0}$	$0.17^{+0.33}_{-0.29}$	4300^{+3110}_{-2780}	$0.7^{+0.4}_{-0.4}$
GW 190926_050336	$62.6^{+18.8}_{-15.3}$	$25.7^{+7.5}_{-6.5}$	$38.9^{+16.1}_{-13.1}$	$23.8^{+9.4}_{-10.1}$	$-0.05^{+0.29}_{-0.33}$	3910^{+2870}_{-2470}	$0.6^{+0.4}_{-0.3}$
GW 191113_103541	$121.6^{+36.1}_{-30.8}$	$36.3^{+13.3}_{-9.7}$	$101.4^{+32.5}_{-29.8}$	$19.5^{+12.6}_{-7.9}$	$0.57^{+0.19}_{-0.20}$	3890^{+3120}_{-2660}	$0.6^{+0.4}_{-0.4}$
GW 191117_023843	$115.0^{+35.3}_{-31.9}$	$38.3^{+9.7}_{-7.9}$	$90.5^{+37.4}_{-31.9}$	$23.6^{+8.5}_{-8.4}$	$-0.18^{+0.27}_{-0.35}$	3510^{+2460}_{-2340}	$0.6^{+0.3}_{-0.3}$
GW 191127_050227	$84.4^{+27.2}_{-21.6}$	$32.3^{+9.5}_{-8.3}$	$57.0^{+30.7}_{-22.3}$	$25.3^{+14.7}_{-12.9}$	$0.24^{+0.32}_{-0.32}$	4200^{+2610}_{-2280}	$0.7^{+0.3}_{-0.3}$
GW 191208_080334	$56.7^{+10.6}_{-10.6}$	$22.7^{+4.1}_{-3.9}$	$37.1^{+12.0}_{-12.3}$	$19.2^{+7.5}_{-6.6}$	$0.13^{+0.29}_{-0.25}$	3020^{+1970}_{-1730}	$0.5^{+0.3}_{-0.3}$
GW 191224_043228	$23.2^{+3.6}_{-3.2}$	$9.3^{+0.9}_{-0.8}$	$15.3^{+4.8}_{-4.8}$	$7.7^{+2.4}_{-2.0}$	$0.09^{+0.15}_{-0.13}$	1670^{+680}_{-740}	$0.3^{+0.1}_{-0.1}$
GW 191228_195619	$239.9^{+132.8}_{-61.3}$	$96.0^{+40.4}_{-31.8}$	$164.6^{+116.3}_{-52.4}$	$78.4^{+37.6}_{-35.9}$	$-0.01^{+0.35}_{-0.38}$	2930^{+2380}_{-1970}	$0.5^{+0.3}_{-0.3}$
GW 200106_134123	$72.2^{+16.5}_{-16.1}$	$29.7^{+7.4}_{-7.2}$	$44.6^{+14.2}_{-13.2}$	$27.2^{+11.8}_{-11.3}$	$0.11^{+0.33}_{-0.30}$	3940^{+2940}_{-2280}	$0.6^{+0.4}_{-0.3}$
GW 200109_195634	$106.9^{+28.7}_{-25.4}$	$44.9^{+12.7}_{-11.7}$	$63.4^{+20.9}_{-18.7}$	$43.6^{+17.8}_{-18.6}$	$0.07^{+0.40}_{-0.38}$	6360^{+4300}_{-3820}	$0.9^{+0.5}_{-0.5}$
GW 200129_114245	$115.9^{+36.3}_{-47.5}$	$43.1^{+16.0}_{-15.6}$	$80.5^{+34.0}_{-41.6}$	$34.2^{+17.4}_{-16.0}$	$0.17^{+0.46}_{-0.41}$	5640^{+4400}_{-3560}	$0.9^{+0.5}_{-0.5}$
GW 200208_211609	$51.3^{+292.4}_{-31.6}$	$21.0^{+35.6}_{-14.5}$	$31.5^{+815.2}_{-15.7}$	$19.4^{+34.6}_{-15.4}$	$0.03^{+0.35}_{-0.34}$	2910^{+3360}_{-2230}	$0.5^{+0.4}_{-0.3}$
GW 200210_005122	$15.2^{+1.9}_{-1.5}$	$6.4^{+0.5}_{-0.4}$	$9.0^{+3.0}_{-2.1}$	$6.0^{+1.5}_{-1.5}$	$0.05^{+0.15}_{-0.10}$	1210^{+500}_{-560}	$0.2^{+0.1}_{-0.1}$
GW 200210_100022	$100.8^{+27.4}_{-24.2}$	$29.1^{+8.9}_{-7.3}$	$85.3^{+26.3}_{-25.2}$	$15.0^{+8.8}_{-5.6}$	$0.63^{+0.30}_{-0.89}$	4950^{+3440}_{-2930}	$0.8^{+0.4}_{-0.4}$
GW 200220_124850	$65.3^{+15.1}_{-13.0}$	$27.7^{+6.7}_{-5.7}$	$38.0^{+10.9}_{-9.9}$	$27.5^{+9.0}_{-9.2}$	$-0.06^{+0.28}_{-0.32}$	4250^{+2700}_{-2570}	$0.7^{+0.4}_{-0.3}$
GW 200214_223307	$81.6^{+28.6}_{-24.6}$	$34.0^{+11.5}_{-10.6}$	$48.9^{+21.8}_{-18.1}$	$32.3^{+14.2}_{-15.0}$	$0.03^{+0.32}_{-0.33}$	5330^{+4210}_{-3580}	$0.8^{+0.5}_{-0.5}$
GW 200225_075134	$100.6^{+19.9}_{-17.6}$	$42.8^{+9.0}_{-7.9}$	$57.7^{+14.4}_{-13.1}$	$43.1^{+13.2}_{-12.8}$	$-0.07^{+0.32}_{-0.36}$	3350^{+2330}_{-2060}	$0.6^{+0.3}_{-0.3}$
GW 200301_211019	$35.2^{+6.5}_{-6.3}$	$14.5^{+2.1}_{-2.1}$	$21.3^{+8.9}_{-6.5}$	$13.3^{+4.3}_{-4.6}$	$-0.12^{+0.23}_{-0.27}$	1980^{+1190}_{-1080}	$0.4^{+0.2}_{-0.2}$
GW 200304_172806	$140.0^{+48.5}_{-45.6}$	$52.6^{+21.9}_{-19.6}$	$94.2^{+49.4}_{-42.3}$	$43.4^{+28.9}_{-29.5}$	$0.39^{+0.44}_{-0.51}$	6610^{+6040}_{-4810}	$1.0^{+0.7}_{-0.6}$
GW 200305_084739	$56.6^{+12.6}_{-10.4}$	$24.0^{+5.6}_{-4.7}$	$32.7^{+9.8}_{-8.4}$	$23.8^{+7.7}_{-8.0}$	$-0.07^{+0.30}_{-0.32}$	4880^{+2510}_{-2800}	$0.8^{+0.3}_{-0.4}$
GW 200318_191337	$76.6^{+18.7}_{-15.8}$	$31.9^{+8.5}_{-6.5}$	$45.4^{+15.2}_{-13.2}$	$30.8^{+12.1}_{-10.8}$	$0.10^{+0.32}_{-0.33}$	6440^{+4140}_{-3750}	$1.0^{+0.5}_{-0.5}$

Table A2. The median, and 90% highest probability density intervals (that is, the narrowest region containing 90% of the posterior probability) for the selected inferred source properties of the signals from O3 analysed in this work. The columns show the total mass of the binary M; the chirp mass $\mathcal{M}$; the component objects' masses m_1, and m_2; the effective inspiral spin; $\chi_{\rm eff}$; the luminosity distance D_L; and the redshift z. All masses are quoted in the source frame, and are derived from inference using the IMRPhenomXPHM BBH waveform model.

(i) **Project-wide defaults**: for example default priors which should normally be applied to all events, information which should be passed to the batch scheduling system being used to perform computation, and information about default.

(ii) **Pipeline defaults**: these apply to all analyses for a given analysis code or pipeline, and will often include sampling settings which are specific to a given analysis code.

(iii) **Event/subject settings** these apply to a single event (or subject) which is to be analysed by Asimov, and will typically include information such as the event time; priors, such as those on the chirp mass which are specific to a given event; and the list of observatories which detected the signal.

(iv) **Analysis-specific settings** which apply only to a single analysis: these will typically include specific setup information, such as the name of the pipeline to be used in this analysis, and the waveform model to be used.

The hierarchical structure allows a substantial reduction in the number of settings which must be curated for each analysis. For example, in this project the majority of analyses were configured using the same analysis-specific blueprint, with only the event-specific blueprints varying substantially between each event.

Asimov blueprints use the YAML serialisation format, and represent a development in the approach used for configuring analyses compared to the one described previously [29], as the method in that work was non-portable and did not allow easy distribution of the configuration data required to reproduce analyses in the manner that blueprint files do. Fuller documentation of blueprint files and their usage can be found in the Asimov documentation [67], along with a number of tutorials.

Appendix B.1. Blueprints used in this work

As a concrete example, we display extracts of the blueprints used in this work in this section. In order to improve the clarity of presentation we have removed some information from these, though the full files are available in the accompanying data release [60].

The first example is our project-wide blueprint. This was applied to our project once, as we were setting it up, and before any events or analyses had been added to the project.

```
kind: configuration
data:
  channels:
    H1: H1:GWOSC-16KHZ_R1_STRAIN
    L1: L1:GWOSC-16KHZ_R1_STRAIN
    V1: V1:GWOSC-16KHZ_R1_STRAIN
  frame types:
    H1: H1:H1_GWOSC_O3b_16KHZ_R1
    L1: L1:L1_GWOSC_O3b_16KHZ_R1
```

```
    V1: V1:V1_GWOSC_O3b_16KHZ_R1
likelihood:
  roll off time: 0.4
postprocessing:
  pesummary:
    cosmology: Planck15
    evolve spins: forwards
    multiprocess: 4
    redshift: exact
    calculate:
    - precessing snr
    skymap samples: 2000
quality:
  state vector:
    L1: L1:GDS-CALIB_STATE_VECTOR_AR
    H1: H1:GDS-CALIB_STATE_VECTOR_AR
    V1: V1:DQ_ANALYSIS_STATE_VECTOR
  minimum frequency:
    H1: 20
    L1: 20
    V1: 20
```

This file contains settings which are not expected to vary between events or analyses, such as the default frame types, and the setup for postprocessing.

Our pipeline specific settings are similarly not expected to change between analyses, but can be used to configure parameters which will be required only for analyses using a specific pipeline; in this instance Bilby and Bayeswave have differing configuration requirements and so are specified as pipeline-specific configurations.

```
kind: configuration
pipelines:

  bilby:
    sampler:
      sampler: dynesty
      kwargs:
        nlive: 1000
        naccept: 60
        sample: acceptance-walk
        check_point_plot: True
        maxmcmc: 100000
      parallel jobs: 3
    scheduler:
```

```
      request cpus: 16
      request disk: 8 #GB
      osg: True
      copy frames: True
    likelihood:
      roll off time: 1
      marginalization:
        time: False
        distance: True

  bayeswave:
    scheduler:
      request memory: 1024
      request post memory: 16384
      copy frames: True
      request disk: 3000000
      osg: True
    likelihood:
      roll off time: 1
      iterations: 100000
      chains: 8
      threads: 4
```

Event-specific settings can then be added in a third blueprint. Unlike the previous two blueprints, which are used once per-project, a different blueprint should be created for each event.

An example blueprint from this project, for GW 200210_005122, is shown below.

```
data:
  segment length: 256
event time: 1265331100.7424316
interferometers: ['H1', 'L1']
kind: event
likelihood:
  psd length: 256
  reference frequency: 20
  sample rate: 8192
  window length: 256
name: GW200210_005122
priors:
  chirp mass:
    maximum: 12
    minimum: 4
```

This blueprint needs to specify the event time, as well as other settings specific to that event, such as the required segment length (which relates to the length of the signal), the chirp mass prior, and the list of interferometers which observed the signal. An event blueprint can typically be created directly from search results, and these can be produced programmatically from the event tables which are published with most catalogues.

Finally, each analysis may be specified in a blueprint. The two main analysis steps in our workflow can be specified in the following minimal blueprints (note that these may be contained in the same file, separated by three hyphen characters). In addition we include the blueprint required to allow Asimov to acquire public data frames as the first "analysis" in the workflow.

```
kind: analysis
name: get-data
pipeline: gwdata
file length: 4096
download:
  - frames
scheduler:
  request memory: 1024
  request post memory: 16384
---
kind: analysis
name: generate-psd
pipeline: bayeswave
comment: Bayeswave on-source PSD estimation process
needs:
  - get-data
---
kind: analysis
name: bilby-IMRPhenomXPHM
pipeline: bilby
waveform:
  approximant: IMRPhenomXPHM

comment: PE job using IMRPhenomXPHM and bilby
needs:
    - generate-psd
```

The dependency structure can be specified by listing the names of analyses which must have completed on a given event in the 'needs' section of the blueprint. The

minimal structure of these files also allows alternative analyses to be created. For example, if an additional run using a second waveform was desired, a copy of the last blueprint could be created, with only the change of waveform approximant name required to configure the extra analysis.